The Astrophysical Journal, 687:141–155, 2008 November 1

THE FATE OF YOUNG RADIO GALAXIES: DECELERATIONS INSIDE HOST GALAXIES?

Nozomu Kawakatu
National Astronomical Observatory of Japan, 2-21-1 Osawa, Mitaka, Tokyo 181-8588, Japan; kawakatu@th.nao.ac.jp

Hiroshi Nagai
National Astronomical Observatory of Japan, 2-21-1, Osawa, Mitaka, Tokyo 181-8588, Japan

and

Motoki Kino
Institute of Space Astronautical Science, JAXA, 3-1-1 Yoshinodai, Sagamihara 229-8510, Japan
Received 2008 May 9; accepted 2008 July 11

ABSTRACT

We examine the evolution of variously sized radio galaxies (i.e., compact symmetric objects [CSOs], medium-size symmetric objects [MSOs], Fanaroff-Riley type II (FR II) radio galaxies by comparing the relation between the hot spot size and the projected linear size with a coevolution model of hot spots and a cocoon. We take account of the deceleration effect by the cocoon head growth. We find that the advance speed of hot spots and lobes inevitably show the deceleration phase (CSO-MSO phase) and the acceleration phase (MSO–FR II phase). This is ascribed to the change of the power-law index of ambient density profile in the MSO phase ($\sim$1 kpc). It is also found that the cocoon shape becomes nearly spherical or disrupted for MSOs, while an elongated morphology is predicted for CSOs and FR II galaxies. This seems to be consistent with the higher fraction of distorted morphology of MSOs than that of CSOs and FR II galaxies. Finally, we predict that only CSOs whose initial advance speed is higher than about 0.1 c can evolve into FR II galaxies, comparing the hot spot speed with the sound speed of the ambient medium.

Subject headings: galaxies: active — galaxies: evolution — galaxies: jets — galaxies: ISM

Online material: color figures

1. INTRODUCTION

According to the standard model for large-scale radio sources (Blandford & Rees 1974), a pair of relativistic jets transport away the bulk kinetic energy from the central compact region close to a central supermassive black hole (SMBH) to $\sim 100-10^3$ kpc scale radio lobes. This bulk kinetic energy is dissipated by the strong terminal shocks which are identified as hot spots. Then, shocked relativistic plasma expands sideways and envelopes the whole jet system and this is a so-called cocoon (Scheuer 1974). Now, how young active galactic nucleus (AGN) jets (or radio sources) evolve into the extended radio sources (e.g., FR II radio galaxies) is one of the primal problems in astrophysics. In order to clarify this issue, it is important to understand the nature of small, young progenitors of FR II galaxies. The study of young progenitor of FR II galaxies is also a good opportunity to get information about the central regions of galaxies, especially their mass density distribution. The coevolution of SMBHs and galaxies has been discussed by many authors who say that AGN feedback may be a key mechanism in regulating the growth of SMBHs and also in preventing further star formation of galaxies; These authors use an analytical approach (e.g., Silk & Rees 1998; King 2003; Wyithe & Loeb 2003; Murray et al. 2005) and a semianalytical approach (e.g., Granato et al. 2004; Kawata & Gibson 2005; Di Matteo et al. 2005; Okamoto et al. 2008). However, it has been unclear how we should treat AGN feedback associated with AGN jets, because we do not understand how small, young radio sources evolve into FR II galaxies. Therefore, for understanding AGN feedback, it is essential to explore conditions under which small, young radio sources can pass through a dense ambient medium within host galaxies.

Recently, a large number of compact, bright double-lobe radio sources, so-called compact symmetric objects (CSOs), whose linear size is $\leq$1 kpc have been discovered (Wilkinson et al. 1994; Fanti et al. 1995; Readhead et al. 1996a, 1996b). Concerning the origin of CSOs, two scenarios were proposed. One is a so-called frustrated jet scenario in which the ambient medium is so dense that the jet cannot break through, so that sources are old and confined (van Breugel et al. 1984). The other is a ''youth radio source scenario'' in which CSOs are the young progenitor of FR II radio galaxies (e.g., Phillips & Mutel 1982). The former scenario looks less likely because recent multiwavelength studies show that the ambient medium of CSOs is not significantly different from FR II radio galaxies (O'Dea1998 and references therein). On the other hand, the most compelling evidence for the youth jet scenario is found in the recent observations of advance speed of hot spots of several CSOs (Owaiank et al. 1998; Taylor et al. 2000; Tschager et al. 2000; Giroletti et al. 2003; Polatidis & Conway 2003; Gugliucci et al. 2005, 2007; Nagai et al. 2006; Luo et al. 2007). They showed that the separation velocity is typically $\sim$0.1 c, indicating a dynamical age of $\sim 10^2-10^4$ yr which implies that CSOs are possible candidates as the progenitors of FR II galaxies.

Based on the youth scenario, the evolution of radio sources has been considered by a number of authors (Carvalho 1985; Begelman & Cioffi 1989; Falle 1991; Fanti et al. 1995; Readhead et al. 1996b; Begelman 1996; De Young 1997; Kaiser & Alexander 1997; Alexander 2000; Snellen et al. 2000; Perucho & Martí 2002; Kawakatu & Kino 2006, hereafter KK06). For simplicity, one has supposed a constant advance speed of hot spots, or a constant aspect ratio of the cocoon (i.e., a self-similar evolution) for a long-term evolution of radio-loud AGNs. *Do these treatments reflect the actual evolution of radio sources*? The answer is not trivial. According to previous observations, a stronger interaction with the ambient medium has been reported for more compact radio sources (e.g., Gelderman & Whittle 1994; de Vries

et al. 1997; Axon et al. 2000; Gupta et al. 2005; Holt et al. 2008). Thus, the advance speed of hot spots might decelerate via the strong interaction in host galaxies. On the evolution of cocoon morphology, recent observations have shown that the fraction of distorted radio morphology of medium-size symmetric objects (MSOs) is higher than CSOs and FR II galaxies (e.g., Saikia et al. 1995; O'Dea 1998; Dallacasa et al. 2002a, 2002b). Observationally, it is unclear whether the assumptions (constant hot spot velocity or constant aspect ratio) are reasonable. Also, the validity of these assumptions is still under debate theoretically (De Young 1997; Komissarov & Falle 1998; O'Dea 1998; Carvalho & O'Dea 2002a, 2002b; Perucho & Martí 2003, hereafter PM03). Therefore, in order to answer the above question, it is essential to build up an appropriate model of radio sources *without assuming the constant aspect ratio and the constant advance speed of hot spots* presented by KK06.

Recently, it has been found that the power-law index for the evolution of hot spot size changes at the transition between the interstellar medium and the intergalactic medium, i.e., $\sim$1–10 kpc (Jeyakumar & Saikia 2000, hereafter JS00; PM03). Since the hot spot is one of the most important ingredients in the whole jet system, the evolution of hot spot size would reflect the dynamical growth of radio sources of various scales. However, it was difficult to derive the dynamical evolution of radio sources from previous work (JS00; PM03) because of the lack of spatial resolution, the observational bias and small sample of radio sources. Therefore, we should not only compile a larger sample of CSOs, MSOs, and FR II radio galaxies, but also be careful about the data quality and the observational bias. Then, from the direct comparison with KK06, we examine the deceleration and acceleration of hot spots.

The paper is organized as follows. In § 2 we first elucidate whether the power-law index change at $\sim$1 kpc is a solid result for the evolution of hot spot size (§ 2.1). To this end, we compile a larger sample of CSOs, MSOs, and FR II sources than previous work (JS00; PM03) by considering the observational bias and being careful about the data quality. We also discuss the advance speed of the hot spot (§ 2.2). In § 3, to interpret these observational data, we briefly review the physical model of hot spot evolution (KK06) with the aid of cocoon dynamics (Kino & Kawakatu 2005, hereafter KK05). In § 4, from the direct comparison with KK06 we reveal the deceleration and acceleration of advance speed of hot spots, and the evolution of cocoon morphology. In § 5 we predict the fate of CSOs by comparing the evolution of hot spot velocity with the sound speed of the ambient medium. Finally, we discuss the FR I/FR II dichotomy and AGN feedback due to the cocoon (i.e., AGN bubble) expansion. Section 6 is devoted to our summary. Throughout this paper we adopt $H_0 = 72$ km s^{-1} Mpc^{-1} and $q_0 = 0.5$.

2. OBSERVATIONAL PROPERTIES OF HOT SPOTS

Following the recent work of Nagai (2007), we compiled variously sized radio galaxies and examined physical quantities of the hot spot (Table 1). FR II sources ($l_h \gtrsim 10$ kpc, where l_h is linear size of radio source) in our sample are selected from FR II radio galaxies in the 3CR catalog (Hardcastle et al. 1998; Fernini et al. 1993; Bridle et al. 1994; Gilbert et al. 2004; Kharb et al. 2008). MSOs ($1 \lesssim l_h \lesssim 10$ kpc) are selected from the samples in Dallacasa et al. (2002a, 2002b). We also included Comact-Steep Spectrum (CSS) sources having double-lobe-like structure in Fanti et al. (1985) and Sanghera et al. (1995) in our MSOs sample. CSOs ($\lesssim$1 kpc) are selected from the samples in Readhead et al. (1996a), Taylor et al. (2000), Wang et al. (2003), Polatidis & Conway (2003), Maness et al. (2004) and Nagai et al. (2006). In addition to these data, we measured hot spot parameters of a CSO (B 1943+546) by analyzing the data obtained from the NASA/IPAC Extragalactic Database (NED). Sources with a complex and highly distorted structure have been excluded from the above samples. To avoid the difference in estimation of physical quantities between the hot spot and the counter hot spot due to the projection effect, we focus on sources with relatively symmetric radio lobes in this work. Finally, we compiled a total of 117 radio sources. For the sources with multiple hot spots, we followed the method of hot spot identification described in the original papers. If there was no information of identification method available in the original papers, we referred to the most prominent component as the hot spot. Based on these data, we investigate how the size of the hot spot changes with the distance from the core in § 2.1. We also discuss the advance speed of the hot spot in § 2.2.

2.1. *Size*

Figure 1 shows the size of a hot spot, $r_{\rm HS}$ with respect to l_h, together with the best linear fit on the log-log plane ($\log y = a \log x + b$). We estimated $r_{\rm HS}$ as $(\theta_{\rm maj} + \theta_{\rm min})/2$, where $\theta_{\rm maj}$ and $\theta_{\rm min}$ are the FWHM of major and minor axes of the component obtained by Gaussian model fittings, respectively. The slope is changed around $\sim$1 kpc, and then the best-fit value of a for $l_h <$ 1 kpc is $a = 1.34 \pm 0.24$, while $a = 0.44 \pm 0.08$ for $l_h > 1$ kpc. This tendency is almost consistent with PM03, but a large number of sources in our sample allow us to confirm the tendency more clearly. One could think the apparent slope change is caused by observational bias. Here we consider the possible uncertainties of the estimation of the hot spot size and the slope change.

First, the sizes of hot spots of larger sources could be underestimated due to a lack of sensitivity for diffuse emission. In this context, there are two major candidates for underestimation of size. One is the missing flux for the diffuse emission due to the absence of a short baseline of the interferometer. Generally, this effect is more serious in VLBI (e.g., VLBA, EVN) observation than in interferometer (e.g., VLA) observation. The hot spot sizes of most sources with $l_h > 1$ kpc are estimated using data taken with VLA while that with $l_h < 1$ kpc are estimated using data taken with VLBI. For the sources with $l_h > 1$ kpc, the missing flux is not significant because almost the total extent of the radio lobe has been, in fact, detected in most sources in our sample. The other candidate is the image dynamic range. Poor dynamic range could contaminate the diffuse emission so that the hot spot sizes could be underestimated. The image dynamic range strongly depends on the distribution of sampled visibilities on the *uv* coverage if we assume each visibility has no significant errors (Perley 1999). Denser and more uniform sampling of visibilities on the *uv* coverage increases the image dynamic range. Thanks to dense and uniform sampling of the visibility, the image dynamic range of VLA observation attains up to several thousands (e.g., Hardcastle et al. 1997), which is much higher than typical VLBI observations. Therefore, we can safely exclude the possibilities of underestimation of the hot spot sizes for larger sources.

Second, the angular resolution relative to the largest angular size of radio source (n_b) possibly affects the estimation of the hot spot size. With high n_b value one could expect to see smaller scale structures within the hot spots, which leads to a decrease in the sizes of hot spots. FR II sources in our sample have observed with n_b that is a few tens of times higher than n_b of CSOs and MSOs in our sample. In this case, smaller scale structure within hot spots could be seen for FR II sources than those of CSOs and MSOs. However, if CSOs and MSOs are observed with the same order of n_b for FR II sources, the hot spot sizes of CSOs

TABLE 1

PHYSICAL PARAMETERS OF HOT SPOTS

			HOT SPOT 1		HOT SPOT 2		
CATALOG	IAU (B1950)	z	θ	Distance	θ	Distance	REFERENCE
(1)	(2)	(3)	(4)	(5)	(6)	(7)	(8)
0013+790	3C 6.1	0.8404	1.8E+03	8.02E+01	2.7E+03	6.98E+01	1
0017+154	3C 9	2.012	2.8E+03	2.94E+01	3.4E+03	4.46E+01	2
0031+391	3C 13	1.351	9.6E+02	9.84E+01	1.2E+03	7.24E+01	1
0034−014	3C 15	0.073	...	...	1.6E+03	2.37E+01	3
0038+32	3C 19	0.482	2.7E+02	1.63E+01	...	...	4
0039+373	...	1.006	2.7E+01	2.96E−01	5.9E+01	2.96E−01	5
0039+391	4C 39.02	1.010	3.2E+02	1.01E+00	2.8E+02	1.01E+00	6
0040+517	3C 20	0.174	4.9E+02	6.39E+01	5.3E+02	6.18E+01	3
0048+5055	3C 22	0.937	2.1E+03	8.57E+01	2.3E+03	6.69E+01	7
0107+315	3C 34	0.69	2.8E+03	1.32E+02	1.8E+03	1.16E+02	1
0108+388	...	0.699	2.6E+00	1.45E−02	1.9E+00	1.81E−02	8
0123+329	3C 41	0.794	1.9E+03	7.15E+01	2.1E+03	6.46E+01	1
0125+287	3C 42	0.395	3.0E+03	5.25E+01	...	...	4
0128+061	3C 44	0.66	1.4E+03	2.19E+02	1.2E+03	1.35E+02	1
0132+37	3C 46	0.437	4.2E+03	4.04E+02	1.8E+04	2.93E+02	4
0133+207	3C 47	0.425	3.8E+03	1.76E+02	...	...	2
0138+136	3C 49	0.621	9.1E+01	2.67E+00	1.9E+02	2.67E+00	9
0152+435	3C 54	0.8274	1.0E+03	1.53E+02	8.1E+02	1.42E+02	1
0154+28	3C 55	0.735	3.0E+03	2.02E+02	3.4E+03	1.96E+02	7
0221+27	3C 67	0.310	<1.3E+03	4.48E+00	1.7E+02	4.48E+00	9
0229+341	3C 68.1	1.238	3.0E+03	1.30E+02	...	...	2
0255+460	...	1.210	4.1E+02	1.97E+00	4.1E+02	1.97E+00	6
0307+169	3C 79	0.256	5.0E+02	1.27E+02	1.5E+03	1.75E+02	3
0316+413	3C 84	0.018	5.7E−01	4.79E−03	6.7E−01	2.98E−03	10
0356+109	3C 98	0.031	2.2E+03	7.74E+01	1.7E+03	9.09E+01	3
0402+379	...	0.055	1.5E+00	9.42E−03	2.4E+00	2.30E−02	1
0404+035	3C 105	0.089	1.9E+03	2.40E+02	3.7E+02	2.65E+02	11
0410+11	3C 109	0.306	4.2E+03	1.67E+02	4.2E+03	1.77E+02	4
0411+141	4C 14.11	0.206	1.9E+03	1.74E+02	5.7E+02	1.09E+02	1
0415+379	3C 111	0.049	9.0E+02	1.11E+02	1.4E+03	6.68E+01	3
0417+177	3C 114	0.815	1.6E+03	1.46E+02	1.3E+03	1.59E+02	1
0429+415	3C 119	0.408	4.7E+01	5.19E−01	8.8E+01	5.19E−01	9
0433+295	3C 123	0.218	3.6E+02	2.27E+01	3.0E+02	2.46E+01	3
0453+227	3C 132	0.214	5.2E+02	3.47E+01	1.0E+03	3.35E+01	3
0511+008	3C 135	0.127	8.3E+02	1.51E+02	6.6E+03	9.38E+01	3
0512+248	3C 136.1	0.064	1.7E+04	2.01E+02	1.4E+04	2.96E+02	3
0528+064	3C 142.1	0.4061	1.3E+03	8.24E+01	1.6E+03	1.54E+02	1
0605+480	3C 153	0.277	4.9E+02	8.74E+00	3.3E+02	1.75E+01	3
0647+452	3C 169.1	0.633	...	1.03E+02	1.7E+03	1.49E+02	1
0651+542	3C 171	0.238	5.6E+02	1.62E+01	7.9E+02	1.52E+01	3
0659+253	3C 172	0.5191	4.4E+03	2.37E+02	1.5E+03	2.68E+02	1
0702+749	3C 173.1	0.292	1.2E+03	9.93E+01	1.4E+03	1.20E+02	3
0707+68	4C 68.08	1.139	8.1E+02	3.52E+00	1.3E+03	3.52E+00	12
0710+118	3C 175	0.768	2.6E+03	1.60E+02	2.5E+03	1.19E+02	2
0710+439	...	0.518	2.1E+00	5.71E−02	5.3E+00	6.49E−02	8
0734+805	3C 184.1	0.118	3.5E+03	2.02E+02	1.4E+03	1.53E+02	3
0802+243	3C 192	0.060	3.8E+03	1.12E+02	1.1E+03	9.66E+01	3
0818+472	3C 197.1	0.130	6.7E+02	1.44E+01	1.2E+03	2.04E+01	3
0822+394	4C 39.23	1.210	2.6E+01	1.50E−01	3.4E+01	1.50E−01	5
0832+14	4C 14.27	0.392	1.1E+03	9.17E+01	...	...	4
0833+654	3C 204	1.112	1.4E+03	7.75E+01	1.4E+03	1.09E+02	2
0850+140	3C 208	1.110	1.3E+03	2.97E+01	1.4E+03	3.85E+01	2
0903+169	3C 215	0.411	1.7E+03	4.61E+01	...	...	2
0917+458	3C 219	0.174	1.8E+03	1.93E+02	6.4E+03	1.94E+02	3
0936+361	3C 223	0.137	5.3E+03	3.09E+02	8.8E+03	3.24E+02	3
0938+399	3C 223.1	0.108	2.5E+03	7.32E+01	1.2E+03	6.99E+01	3
0939+140	3C 225	0.582	2.6E+02	1.18E+01	2.6E+02	8.72E+00	4
0945+076	3C 227	0.086	1.1E+03	1.63E+02	1.1E+03	1.64E+02	3
0947+145	3C 228	0.552	1.2E+03	1.23E+02	...	1.10E+02	4
0958+290	3C 234	0.185	9.8E+02	1.77E+02	1.5E+03	1.31E+02	3
1005+07	3C 237	0.877	8.7E+02	2.35E+00	8.7E+02	2.35E+00	13
1019+22	3C 241	1.617	2.8E+02	2.65E+00	2.7E+02	2.65E+00	9

TABLE 1—*Continued*

			Hot Spot 1		Hot Spot 2		
Catalog	IAU (B1950)	z	θ	Distance	θ	Distance	Reference
(1)	(2)	(3)	(4)	(5)	(6)	(7)	(8)
1030+585	3C 244.1	0.428	1.3E+03	1.15E+02	9.2E+02	8.60E+01	4
1031+567	...	0.460	2.8E+00	8.05E−02	3.4E+00	8.14E−02	14
1100+772	3C 249.1	0.311	4.6E+03	7.34E+02	1.3E+03	2.99E+01	2
1137+660	3C 263	0.646	1.7E+03	1.13E+02	1.5E+03	8.80E+01	2
1142+31	3C 265	0.811	5.6E+03	2.68E+02	3.2E+03	1.72E+02	7
1143+50	3C 266	1.275	1.8E+03	1.24E+01	3.0E+03	1.24E+01	13
1159+394	...	2.370	2.3E+01	1.36E−01	3.1E+01	1.36E−01	5
1203+645	3C 268.3	0.371	9.5E+01	3.35E+00	<1.2E+03	3.35E+00	9
1225+442	...	0.348	8.7E+01	4.16E−01	8.9E+01	4.16E−01	5
1232+216	3C 274.1	0.422	4.6E+03	3.58E+02	4.6E+03	3.27E+02	4
1244+49	4C 49.25	0.206	5.8E+02	3.02E+00	3.2E+02	4.87E+00	5
1250+56	3C 277.1	0.321	<1.3E+03	5.17E+00	<8.5E+02	1.59E+00	12
1308+277	3C 284	0.239	3.7E+03	3.45E+02	2.2E+03	2.40E+02	3
1314+453	...	1.544	1.3E+02	4.74E−01	1.3E+02	4.74E−01	5
1319+428	3C 285	0.079	3.5E+03	1.11E+02	1.1E+04	1.30E+02	3
1343+386	4C 38.37	1.844	3.5E+01	3.18E−01	1.2E+01	3.18E−01	5
1404+286	OQ 208	0.077	4.1E−01	5.15E−03	6.4E−01	5.15E−03	15
1419+419	3C 299	0.367	2.1E+02	1.64E+01	2.1E+02	2.39E+01	4
1420+198	3C 300	0.272	1.1E+03	2.51E+02	1.3E+03	1.05E+02	1
1441+522	3C 303	0.141	3.2E+03	3.82E+01	1.6E+03	3.82E+01	3
1443+77	3C 303.1	0.267	5.3E+02	3.20E+00	2.3E+03	3.20E+00	13
1447+77	3C 305.1	1.132	1.5E+03	5.97E+00	2.4E+03	5.97E+00	13
1522+546	3C 319	0.192	3.3E+03	1.36E+02	...	...	3
1559+021	3C 327	0.104	6.2E+02	3.21E+02	1.2E+03	1.75E+02	3
1607+268	CTD 93	0.473	7.5E+00	1.22E−01	1.1E+01	1.22E−01	16
1609+660	3C 330	0.550	1.3E+03	1.44E+02	...	...	4
1618+177	3C 334	0.555	2.7E+03	1.01E+02	...	...	2
1622+238	3C 336	0.927	4.8E+03	5.58E+02	4.8E+03	8.95E+01	2
1626+27	3C 341	0.448	1.1E+03	1.70E+02	...	...	4
1637+624	3C 343.1	0.750	<7.9E+02	1.07E+00	<5.6E+02	1.07E+00	9
1658+471	3C 349	0.205	1.2E+03	1.20E+02	1.7E+03	1.28E+02	3
1704+608	3C 351	0.371	1.1E+03	8.64E+02	...	...	2
1717+009	3C 353	0.030	2.0E+03	5.50E+01	1.5E+03	7.17E+01	3
1723+510	3C 356	1.079	3.5E+03	2.98E+02	3.0E+03	1.49E+02	7
1832+474	3C 381	0.161	4.6E+02	8.11E+01	1.5E+03	8.86E+01	3
1833+326	3C 382	0.058	2.2E+03	9.15E+01	2.3E+03	8.72E+01	3
1842+455	3C 388	0.091	3.5E+03	2.50E+01	1.7E+03	2.58E+01	3
1845+797	3C 390.3	0.056	1.9E+03	1.07E+02	3.1E+03	9.10E+01	3
1939+605	3C 401	0.201	1.5E+03	2.59E+01	1.2E+03	3.62E+01	3
1943+546	...	0.263	7.3E+00	8.96E−02	6.8E+00	5.27E−02	10
1949+023	3C 403	0.059	3.3E+02	3.07E+01	2.6E+03	5.15E+01	3
1957+405	3C 405	0.057	5.0E+02	6.55E+01	7.6E+02	5.50E+01	3
2045+068	3C 424	0.127	3.6E+02	1.81E+01	7.3E+02	8.74E+00	3
2104+763	3C 427.1	0.572	2.3E+03	4.81E+01	2.3E+03	5.41E+01	4
2120+168	3C 432	1.805	1.4E+03	3.31E+01	1.4E+03	4.42E+01	2
2121+248	3C 433	0.102	...	...	1.0E+03	1.06E+01	3
2141+279	3C 436	0.215	4.9E+03	1.77E+02	8.5E+02	1.34E+02	3
2153+377	3C 438	0.290	7.5E+02	4.27E+01	7.5E+02	3.33E+01	3
2203+292	3C 441	0.707	1.3E+03	5.37E+01	1.3E+03	1.31E+02	1
2221-021	3C 445	0.056	1.7E+03	3.00E+02	2.6E+03	2.84E+02	3
2243+394	3C 452	0.081	3.4E+03	1.86E+02	1.3E+03	1.80E+02	3
2309+184	3C 457	0.428	4.6E+03	4.78E+02	1.2E+03	4.14E+02	4
2352+495	...	0.237	3.3E+00	7.95E−02	5.5E+00	8.34E−02	8
2352+796	3C 469.1	1.336	2.2E+03	2.18E+02	4.0E+03	2.33E+02	1
2356+437	3C 470	1.653	1.3E+03	8.44E+01	1.2E+03	6.20E+01	1

Notes.—Col. (1): Source name in IAU format (B1950). Col. (2): Catalog name. Col (3): Redshift. Cols. (4) and (6): θ is the size of the hot spot (pc). Cols. (5) and (7): Hot spot distance from the core (kpc); if the core is not visible in the image, we give the distance as a half of the separation between the hot spot and the counter hot spot. Col. (8): References.

References.—(1) Kharb et al. 2008; (2) Bridle et al. 1994; (3) Hardcastle et al. 1998; (4) Gilbert et al. 2004; (5) Dallacasa et al. 2002a; (6) Dallacasa et al. 2002b; (7) Fernini e al. 1993; (8) Readhead et al. 1996b; (9) Fanti et al. 1985; (10) this paper; (11) Maness et al. 2004; (12) Sanghera et al. 1995; (13) Spencer et al. 1989; (14) Taylor et al. 2000; (15) Wang et al. 2003; (16) Nagai et al. 2006.

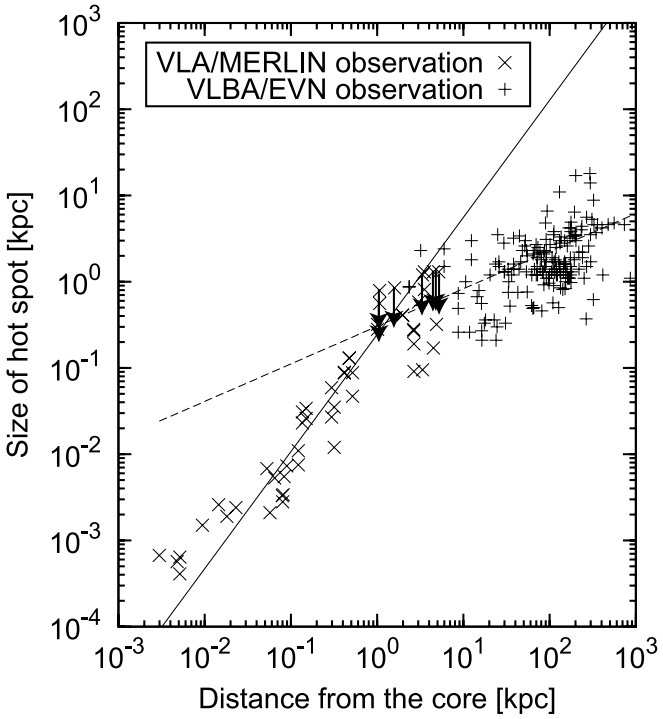

FIG. 1.—Relation of hot spot size ($r_{\rm HS}$) and hot spot distance from the core (l_h). Crosses with arrows indicate the upper limit. The solid line corresponds to the best-fit for the sources where 10^{-3} kpc $\leq l_h \leq 1$ kpc, whereas the dashed line corresponds to that for the sources where 1 kpc $\leq l_h \leq 10^3$ kpc. Note that upper limit data were not included in the fittings.

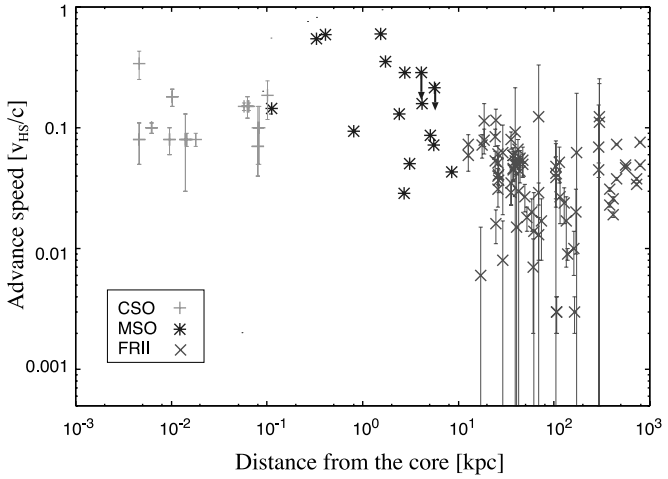

FIG. 2.—Relation of hot spot velocity ($v_{\rm HS}$) and hot spot distance from the core (l_h). Plus signs, stars, and crosses represent CSOs, MSOs, and FR II radio galaxies, respectively. [*See the electronic edition of the Journal for a color version of this figure*.]

and MSOs should decrease. This effect is more serious in smaller sources. As a result, the slope in CSO-MSO phase would be more inverted ($a > 1.34 \pm 0.02$) but the starting point of slope change would be unchanged. Intensive study by JS00 found a similar change in slope, but the change occurred around ~20 kpc. They selected the sample observed with similar n_b among CSOs, MSOs, and FR II sources. However, their sample contains many FR II sources for which the hot spot sizes have been determined as only upper limits due to lack of angular resolution. This would make the starting point of the slope change unclear.

Finally, we comment on the projection effect. To be precise, our estimated size of the hot spot is not intrinsic size but the size projected onto the celestial plane. However, our sample was restricted to the sources with relatively symmetric lobes. We excluded the one-sided sources. Thus the difference in the jet axis is not so large among the sources, and affects the estimation of the size by no more than a factor of a few.

Overall, even if we allow for possible uncertainties discussed above, the trend of the $r_{\rm HS}$-l_h relation would not be changed. It seems reasonable to suppose that the slope change occurs around 1 kpc.

2.2. *Advance Speed*

Figure 2 shows the advance speed of hot spots ($v_{\rm HS}$). For CSOs, $v_{\rm HS}$ has been directly measured by VLBI observations. In the case of CSOs where the hot spot motion was measured relative to the counter hot spot (so-called the separation rate, $v_{\rm sep}$), we estimated $v_{\rm HS}$ as $v_{\rm sep}/2$. On the other hand, the $v_{\rm HS}$ of FR II sources has not been measured directly. We therefore adopted the $v_{\rm HS}$ of MSOs and FR II sources estimated by the synchrotron age constraints (Alexander et al. 1984; Carilli et al. 1991; Liu et al. 1992; Klein et al. 1995; Mack et al. 1998; Parma et al. 1999; Murgia et al. 1999; Schoenmakers et al. 2000; Jamrozy et al. 2005), which is estimated by the break frequency of radio spectra caused by the synchrotron aging. We adopted the $v_{\rm HS}$ of MSOs only from the lobe-dominated source (classified type A in Murgia et al. 1999). We summarize the data of $v_{\rm HS}$ in Table 2.

As we show in the following, there are a number of biases and uncertainties in the estimation of $v_{\rm HS}$. We should conclude that the evolution of $v_{\rm HS}$ relative to l_h is not clear at this moment. We do not therefore argue in favor of the evolutionary model based on the observational data of $v_{\rm HS}$.

First, the apparent absence of CSOs with $v_{\rm HS} <\sim 0.1c$ is possibly due to the observational biases. In Figure 3 we show the apparent velocity of the hot spots of CSOs with respect to redshift of the source. Each parameter is listed in Table 3. Apparent velocity of less than ~10 μas yr^{-1} has not been detected. This is probably due to a lack of angular resolution. Apparent velocity of ~10 μas yr^{-1} corresponds to ~0.1 c in $z > 0.1$, so that it is possible to conclude that the apparent absence of $v_{\rm HS} < 0.1c$ in CSOs is due to biases introduced by the detection limits.

Second, the synchrotron age estimates are more uncertain than the kinematic age estimates. Primary uncertainty in the estimation of synchrotron age is the magnetic field. Although the minimum-energy condition is highly uncertain, the minimum-energy field is usually adopted due to the lack of better estimation. Since the synchrotron age strongly depends on the magnetic field rather than the break frequency ($t_{\rm syn} \propto B^{-1.5}\nu_b^{-0.5}$), uncertainty of magnetic field makes it difficult to relate the source age. Therefore, $v_{\rm HS}$ of MSOs and FR II sources are more unreliable than that of CSOs.

Finally, a direct comparison of $v_{\rm HS}$ between MSOs and FR II sources is not acceptable because the estimation method of $v_{\rm HS}$ is different between MSOs and FR II sources. Basically, $v_{\rm HS}$ of FR II sources is calculated by the linear fit to the observed synchrotron age distribution across the lobe as $v_{\rm HS}$ of FR II sources (cf. Fig. 3 in Alexander et al. 1984). On the other hand, the advance velocities of MSOs in Murgia et al. (1999) are estimated in a different way. Murgia et al. calculated the break frequency by fitting the integrated spectra to the continuous injection model (CI model). Then they estimated $v_{\rm HS}$ as $l_h/t_{\rm CI}$, where $t_{\rm CI}$ is the synchrotron age estimated from the break frequency of the CI model spectrum. The main concern of this method is that the integrated spectrum could contain not only the lobe emission but also the core and jet emission. To be precise, the estimated synchrotron age is the mean particle age of these components. The electrons

TABLE 2

ADVANCE SPEED OF HOT SPOTS

			HOT SPOT 1		HOT SPOT 2		
SOURCE (1)	CATALOG (2)	z (3)	Distance (4)	β (5)	Distance (6)	β (7)	REFERENCE (8)
0035+227	...	0.096	1.41E−02	0.078 ± 0.055	1.41E−02	0.078 ± 0.055	1
0108+388	...	0.668	1.45E−02	0.084 ± 0.007	1.81E−02	0.084 ± 0.007	2
0109+492	...	0.067	3.82E+02	0.031 ± 0.001	3.82E+02	0.023 ± 0.001	3
0145+532	3C 52	0.285	7.34E+01	0.017 ± 0.009	5.87E+01	0.020 ± 0.006	4
0221+276	3C 67	0.310	4.73E+00	0.16	4.73E+00	0.16	5
0316+413	3C 84	0.018	4.61E−03	0.340 ± 0.090	...	...	6
0403+768	...	0.599	3.68E−01	0.55	3.68E−01	0.55	5
0404+428	3C 103	0.330	1.05E+02	0.039 ± 0.039	1.13E+02	0.052 ± 0.017	4
0512+249	3C 136.1	0.064	1.69E+02	0.020 ± 0.011	1.15E+02	0.027 ± 0.011	4
0538+498	3C 247	0.749	3.71E+01	0.059 ± 0.005	3.71E+01	0.045 ± 0.009	7
0610+260	3C 154	0.580	1.07E+02	0.003 ± 0.001	1.07E+02	0.003 ± 0.001	4
0640+233	3C 165	0.296	1.62E+02	0.010 ± 0.004	1.35E+02	0.017 ± 0.010	4
0642+214	3C 166	0.245	6.88E+01	0.013 ± 0.005	6.88E+01	0.029 ± 0.006	4
0710+439	...	0.518	5.76E−02	0.152 ± 0.014	6.50E−02	0.152 ± 0.014	8
0740+380	3C 186	1.067	5.70E+00	0.09	5.70E+00	0.09	5
0813+758	...	0.232	7.99E+02	0.076 ± 0.001	7.99E+02	0.049 ± 0.001	3
0958+290	2C 234	0.185	3.90E+01	0.092 ± 0.122	2.90E+01	0.062 ± 0.043	4
1003+351	...	0.101	1.98E+03	0.120 ± 0.001	...	...	3
1005+077	3C 237	0.877	3.13E+00	0.29	3.13E+00	0.29	5
1008+467	3C 239	1.781	2.57E+01	0.031 ± 0.009	2.57E+01	0.040 ± 0.006	7
1019+222	3C 241	1.617	1.95E+00	0.35	1.95E+00	0.35	5
1030+585	3C 244.1	0.428	1.04E+02	0.048 ± 0.026	1.04E+02	0.042 ± 0.016	4
1031+567	...	0.450	7.95E−02	0.099 ± 0.052	8.34E−02	0.099 ± 0.052	9
1040+123	3C 245	1.029	1.77E+01	0.072 ± 0.016	...	...	7
1111+408	3C 254	0.736	3.76E+01	0.046 ± 0.009	3.76E+01	0.059 ± 0.009	7
1140+223	3C 263.1	0.824	1.86E+01	0.114 ± 0.044	1.86E+01	0.079 ± 0.018	7
1142+318	3C 265	0.811	1.73E+02	0.062 ± 0.132	...	...	4
1143+500	3C 266	1.275	1.27E+01	0.059 ± 0.015	1.27E+01	0.073 ± 0.015	7
1153+317	...	0.417	9.00E−01	0.56	9.00E−01	0.56	5
1203+645	3C 268.3	0.371	2.57E+00	0.13	2.57E+00	0.13	5
1206+439	3C 268.4	1.398	2.44E+01	0.084 ± 0.014	2.44E+01	0.053 ± 0.011	7
1209+745	...	0.107	4.17E+02	0.026 ± 0.001	4.17E+02	0.019 ± 0.001	3
1218+339	3C 270.1	1.532	2.60E+01	0.061 ± 0.010	2.60E+01	0.051 ± 0.010	7
1233+216	3C 274.1	0.422	2.93E+02	0.045 ± 0.006	2.93E+02	0.069 ± 0.085	4
1241+166	3C 275.1	0.555	4.68E+01	0.050 ± 0.010	4.68E+01	0.054 ± 0.015	7
1245+676	...	0.107	6.17E−03	0.103 ± 0.009	6.17E−03	0.103 ± 0.009	10
1250+568	3C 277.1	0.320	3.06E+00	0.03	3.06E+00	0.03	5
1251+159	3C 277.2	0.766	1.28E+02	0.024 ± 0.008	...	...	4
1254+476	3C 280	0.996	3.93E+01	0.049 ± 0.008	3.93E+01	0.053 ± 0.008	7
1308+277	3C 284	0.239	4.27E+01	0.030 ± 0.035	6.14E+01	0.014 ± 0.015	4
1312+698	...	0.106	4.51E+02	0.073 ± 0.001	4.51E+02	0.038 ± 0.001	3
1319+428	3C 285	0.079	5.17E+01	0.018 ± 0.004	6.06E+01	0.007 ± 0.005	4
1323+321	...	0.370	1.25E−01	0.14	1.25E−01	0.14	5
1336+391	3C 288	0.246	3.53E+01	0.029 ± 0.006	3.53E+01	0.035 ± 0.012	7
1340+381	...	0.229	1.09E+03	0.112 ± 0.030	1.09E+03	0.085 ± 0.038	2
1343+500	3C 289	0.967	2.64E+01	0.041 ± 0.008	2.64E+01	0.037 ± 0.008	7
1349+647	2C 292	0.710	2.96E+02	0.111 ± 0.120	2.96E+02	0.124 ± 0.132	4
1350+316	3C 293	0.045	6.95E+01	0.123 ± 0.209	...	...	4
1404+286	OQ 208	0.077	4.60E−03	0.080 ± 0.050	4.60E−03	0.080 ± 0.050	11
1404+344	3C 294	1.779	4.39E+01	0.044 ± 0.009	4.39E+01	0.056 ± 0.009	7
1416+067	3C 298	1.437	6.32E+00	<0.22	6.32E+00	<0.22	5
1419+419	3C 299	0.367	2.46E+01	0.115 ± 0.027	2.46E+01	0.016 ± 0.005	7
1420+198	3C 300	0.270	1.70E+01	0.006 ± 0.009	4.04E+01	0.015 ± 0.026	4
1443+773	3C 303.1	0.267	3.48E+00	0.05	3.48E+00	0.05	5
1447+771	3C 305.1	1.132	6.26E+00	0.07	6.26E+00	0.07	5
1502+262	3C 310	0.054	1.38E+02	0.009 ± 0.001	1.63E+02	0.003 ± 0.001	4
1522+546	3C 319	0.192	2.90E+01	0.008 ± 0.009	...	...	4
1543+845	...	0.201	7.29E+02	0.038 ± 0.001	7.29E+02	0.034 ± 0.001	3
1607+268	CTD 93	0.473	1.10E−01	0.170 ± 0.060	1.10E−01	0.170 ± 0.060	12
1637+626	3C 343.1	0.750	9.04E−01	0.09	9.04E−01	0.09	5
1843+356	...	0.764	1.02E−02	0.180 ± 0.025	1.02E−02	0.180 ± 0.025	2
1943+546	...	0.263	6.23E−02	0.151 ± 0.033	6.23E−02	0.151 ± 0.033	1

TABLE 2—*Continued*

Source (1)	Catalog (2)	z (3)	Hot Spot 1 Distance (4)	Hot Spot 1 β (5)	Hot Spot 2 Distance (6)	Hot Spot 2 β (7)	Reference (8)
1957+4035	3C 405	0.056	3.54E+01	0.080 ± 0.013	4.21E+01	0.067 ± 0.013	13
2043+749	...	0.104	5.56E+02	0.047 ± 0.001	5.56E+02	0.049 ± 0.001	3
2117+605	3C 430	0.056	4.92E+01	0.027 ± 0.007	...	...	4
2248+712	3C 454.1	1.841	4.59E+00	<0.29	4.59E+00	<0.29	5
2252+129	3C 455	0.543	9.52E+00	0.04	9.52E+00	0.04	5
2342+821	...	0.735	4.59E+00	0.59	4.59E+00	0.59	5
2352+495	...	0.238	8.05E−02	0.071 ± 0.025	8.05E−02	0.071 ± 0.025	1

Notes.—Col. (1): Source name in IAU format (B1950). Col. (2): Catalog name. Col (3): Redshift. Cols. (4) and (6): Hot spot distance from the core (kpc). Cols. (5) and (7): β is the advance velocity of hot spot ($v_{\rm HS}/c$). Advance velocities of CSOs are calculated as $v_{\rm HS} = v_{\rm sep}/2$, where $v_{\rm sep}$ is the separation rate between hot spots, except for 3C 84. This is because the advance velocity is not measured directly in most CSOs. We estimated the hot-spot distance (l_h) as a half-length between the hot spots for the sources whose l_h is not specified in the literature. Also, we adopted a half-length between hot spots for l_h of CSOs where the core has not identified. Col. (8): References.

References.—(1) Polatidis & Conway 2003; (2) Jamrozy et al. 2005; (3) Schoenmakers et al. 2000; (4) Alexander & Leahy. (1987); (5) Murgia et al. 1999; (6) Asada et al. 2006; (7) Liu et al. 1992; (8) Owsianil & Conway 1998; (9) Taylor et al. 2000; (10) Marecki et al. 2003; (11) Wang et al. 2003; (12) Nagai et al. 2006; (13) Carilli et al. 1991.

in the core and jets, especially in the knots of the jets, are likely to be sites of particle acceleration. Thus the estimated synchrotron age could be underestimated compared to actual source age, which leads to the overestimation of $v_{\rm HS}$.

3. A COEVOLUTION MODEL OF HOT SPOTS AND A COCOON

In this section we briefly review a dynamical evolution model of radio sources (KK06) which traces the dynamical evolution of advancing hot spots and expanding cocoons (e.g., Begelman & Cioffi 1989; see also KK05). Hereafter, the mass, momentum, and kinetic energy of unshocked jet flow are conserved. In other words, we do not consider the entrainment effect of the ambient medium. This would be justified for the relativistic jet flows (e.g., Scheck et al. 2002, hereafter S02; Mizuta et al. 2004).

The basic equations of the cocoon expansion can be obtained as follows:

1. The equation of motion along the jet axis, i.e., the momentum flux of a relativistic jet, is balanced to the ram pressure of the ambient medium spread over the effective cross-section area of the cocoon head, A_h,

$$L_j/c = \rho_a v_{\rm HS}^2 A_h,$$

where L_j, ρ_a, and $v_{\rm HS}$ are the total kinetic energy of jets, the mass density of the ambient medium and the hot spot velocity, respectively. Here we assume that L_j is constant in time, and that $v_{\rm HS} = v_h$, where v_h is the advance speed of the cocoon head (see KK06 for details).

2. The equation of motion perpendicular to the jet axis, that is, the sideways expansion velocity, v_c is equal to the shock speed driven by the overpressured cocoon with the internal pressure, P_c,

$$P_c = \rho_a v_c^2.$$

For CSOs, the sideways expansion velocity evaluated by the outflow velocity of the line-emitting gas (e.g., de Vries et al. 1999; Axon et al. 2000; O'Dea et al. 2002; Gupta et al. 2005; Holt et al. 2008) would be higher than the sound velocity of the ambient medium. Even for FR II galaxies, the overpressured expansion would be valid (e.g., KK05; Ito et al. 2008).

3. The energy conservation in the cocoon, namely, all of the kinetic energy transported by jets during the source age t, is deposited as the cocoon's internal pressure,

$$P_c V_c = 2(\gamma_c - 1) L_j t,$$

where V_c is the volume of the cocoon and $\gamma_c = 4/3$ is the specific heat ratio of the relativistic plasma in the cocoon.

For simplicity, we do not consider the bremsstrahlung cooling of the cocoon, although this would be important in the much earlier phase of the evolution (Kino et al. 2007).

According to KK06, the physical quantities of hot spots and the cocoon can be determined by the mass density of the ambient medium, ρ_a and the cross-section area of the cocoon body, A_c (see Fig. 4). The mass density profile is expressed as

$$\rho_a(d) \propto d^{-\alpha},$$

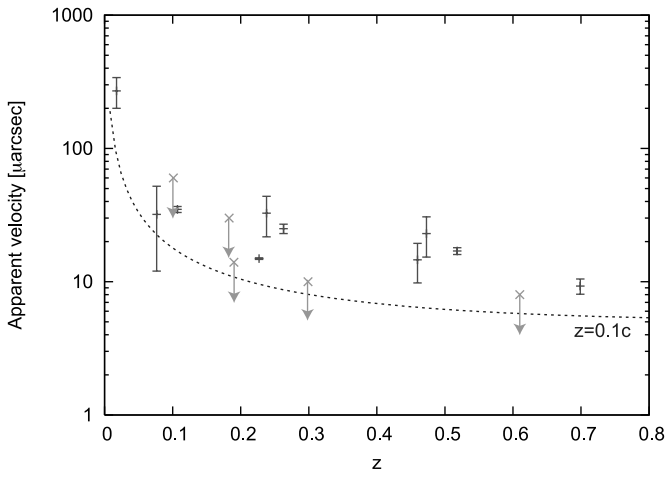

Fig. 3.—Apparent separation velocity between hot spots of CSOs. Arrows indicate upper limits (Taylor & Vermeulen 1997; Gugliucci et al. 2005). Concerning the sources in Gugliucci et al. (2005), we have not adopted J1415+13 because the separation rate is measured not between hot spots but jet components. The dashed line corresponds to the velocity 0.1 c. [*See the electronic edition of the Journal for a color version of this figure.*]

TABLE 3
APPARENT SEPARATION RATE (v_{app}) BETWEEN HOT SPOTS

Source	z	v_{app} (μas)	Reference
0108+388	0.699	9.27 ± 1.21	1
0710+439	0.518	17 ± 1	2
1031+567	0.4597	14.6 ± 4.8	3
1245+676	0.1071	34.9 ± 1.8	4
1943+546	0.263	25 ± 2	2
2352+495	0.238	32.7 ± 11	3
OQ208	0.0766	32 ± 20	5
CTD93	0.473	23 ± 7.7	6
3C 84[a]	0.0183	270 ± 70	7
J1111+1955	0.299	<10	8
J1414+4554	0.19	<14	8
J1734+0926	0.61	<8	8
1946+708	0.101	<60	9
J1934−638[a]	0.183	<30	10

[a] We measure v_{app} between the core and hot spot.

REFERENCES.—(1) Owsianik et al. 1998; (2) Polatidis & Conway 2003; (3) Taylor et al. 2000; (4) Marecki et al. 2003; (5) Wang et al. 2003; (6) Nagai et al. 2006; (7) Asada et al. 2006; (8) Gugliucci et al. 2005; (9) Taylor & Vermeulen 1997; (10) Tzioumis et al. 1989.

where d is the radial distance from the center of the galaxy. The cross-sectional area of the cocoon body is given by

$$A_c(t) = \pi l_c^2 \propto t^X,$$

where $l_c = \int_{t_{\min}}^{t} v_c(t')dt'$ is the radius of the cocoon body. Here $t_{\min}$ is the time from when the two-dimensional (2D) phase (A_h growth phase) starts. On a free parameter X, we can constrain the value of X, in comparison with numerical simulations. We will discuss this issue later. Assuming that A_h/r_{HS}^2 is constant in time, the quantities of hot spots (r_{HS}, v_{HS} and P_{HS}) can be described in terms of the length from the center of the galaxy to the hot spot (l_h) as follows:

$$r_{HS} \propto l_h^{\frac{X(-2+0.5\alpha)(\alpha-2)+3\alpha-4}{2X(-2+0.5\alpha)+6}} \propto l_h^{S_r}, \quad (1)$$

$$v_{HS} \propto l_h^{\frac{2-X(2-0.5\alpha)}{X(-2+0.5\alpha)+3}} \propto l_h^{S_v}, \quad (2)$$

$$P_{HS} \propto l_h^{\frac{X(2-0.5\alpha)(\alpha-2)+4-3\alpha}{X(-2+0.5\alpha)+3}} \propto l_h^{S_p}, \quad (3)$$

where S_r, S_v, and S_p represent the values of the exponents of the hot spot radius, advance velocity, and pressure, respectively. We apply the conditions of $Y \equiv X(-2 + 0.5\alpha) + 3 > 0$, which make the contribution at $t_{\min}$ in the integration of $l_h = \int_{t_{\min}}^{t} v_{HS}(t')dt' \propto t^Y - t_{\min}^Y$ small enough. In other words, we do not consider the case that the lifetimes of compact radio sources are much longer than those of extended radio sources because this is unrealistic.

Here, let us consider the α and X dependence on the advance velocity of hot spots for fixed physical quantities at $t = t_{\min}$. Concerning α dependence in fixed X, larger α leads to a weaker deceleration effect on v_{HS} due to smaller ρ_a. Also, in order to keep the constant velocity of sideways expansion, larger α predicts smaller cocoon pressure P_c because of $P_c = \rho_a v_c^2$. Next we consider the X dependence. Larger X leads to larger A_c and v_c, and thus the larger P_c is required because of $P_c = \rho_a v_c^2$. Thus, the slower v_{HS} is needed in order to satisfy the energy conservation in the cocoon, that is, $P_c A_c v_{HS} = \text{const}$. In summary, larger (smaller) α and smaller (larger) X leads to acceleration (deceleration) of hot spot velocity.

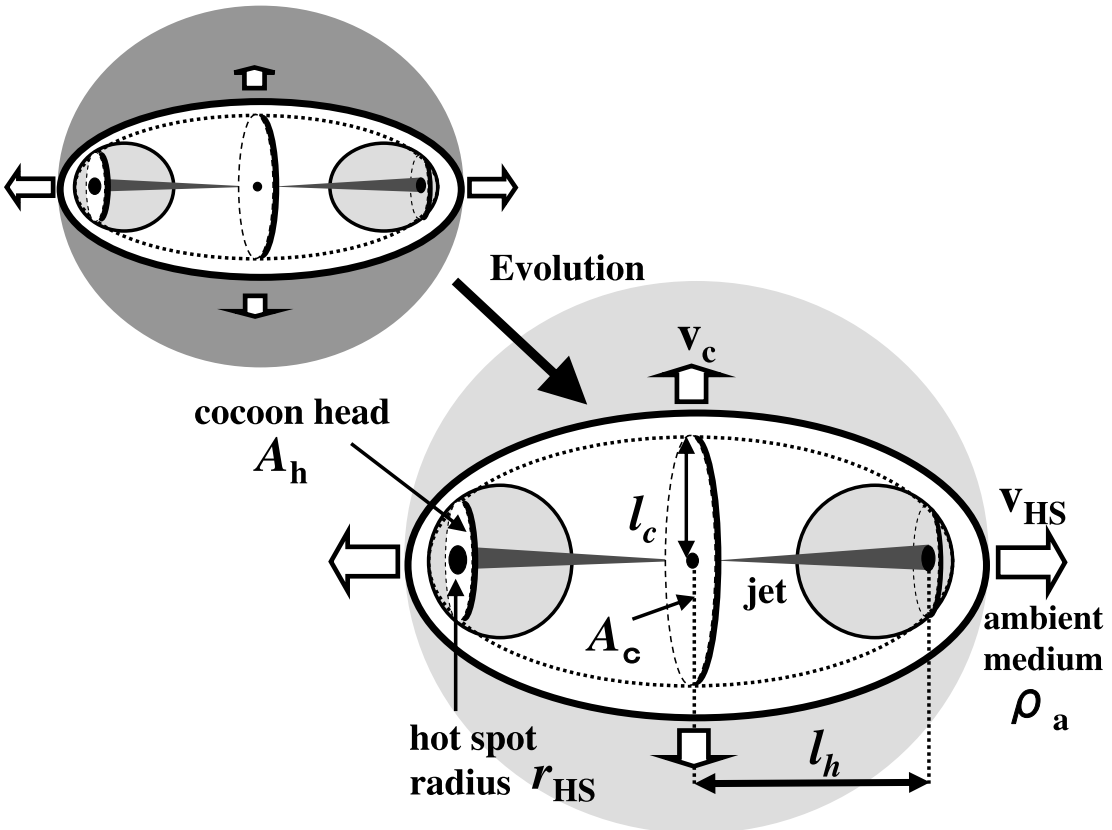

FIG. 4.—Schematic picture of the evolution of radio sources. The aspect ratio of the cocoon is defined as $\mathcal{R} = l_c/l_h$.

TABLE 4
Comparison with 2D Relativistic Hydrodynamic Simulations

Model	$v_{\rm HS}$	$r_{\rm HS}$	$P_{\rm HS}$
(1) A Uniform Ambient Medium ($\alpha = 0$)			
S02	$l_h^{-0.55}$	$l_h^{0.45}$	$l_h^{-1.1}$
KK06	$l_h^{-0.56}$	$l_h^{0.55}$	$l_h^{-1.1}$
(2) A Declining Ambient Medium ($\alpha = 1$)			
PM07	$l_h^{-0.11}$	$l_h^{0.78}$	$l_h^{-1.4}$
KK06	$l_h^{-0.11}$	$l_h^{0.67}$	$l_h^{-1.2}$

Note.—Case 1 corresponds to KK06 model with $X = 1.2$, while case 2 corresponds to KK06 model with $X = 1.4$.

The aspect ratio of the cocoon, $\mathcal{R} \equiv l_c/l_h$, is also an important quantity relevant to the evolution of radio galaxies. The l_h-dependence of the aspect ratio of cocoon is then given by

$$\mathcal{R} \propto l_h^{\frac{X(2.5-0.5\alpha)-3}{X(-2+0.5\alpha)+3}} \propto l_h^{S_R}. \quad (4)$$

Finally, in order to check the reliability of their analytical model, we compare the results of KK06 compared with 2D relativistic hydrodynamic simulations in a uniform ambient medium with $\alpha = 0$ (S02) and in a declining ambient medium with $\alpha = 1$ (Perucho & Martí 2007, hereafter PM07). We summarize the comparisons with 2D hydrodynamic simulations in Table 4. These results show that the analytic model (KK06) can well agree with the results of 2D simulations. Thus, it is possible to constrain the free parameter X by direct comparison with numerical simulations. Following the results of S02 and PM07, we can constrain $1.2 \leq X \leq 1.4$ for the wide range of α(=0–2.5) because X does not depend on α significantly (see Table 4). As seen in Table 4 we find that the power-law index of $r_{\rm HS}$ is slightly different from the results of KK06 and those of numerical simulations (S02 and PM07).[1] However, such small deviations do not affect the following results.

4. WHAT CAN WE LEARN FROM OBSERVED $r_{\rm HS}$-l_h RELATION?

In this section we examine the deceleration and acceleration of hot spot velocity by comparing the observed $r_{\rm HS}$-l_h relation with the KK06 model.

4.1. *Constant Velocity Model or Constant Aspect Ratio Model?*

Here we test two well-known evolution scenarios of radio sources, that is, (1) the constant velocity model ($v_{\rm HS} = $ const) proposed by Readhead et al. (1996b), and (2) the self-similar model with $\mathcal{R} = $ const (e.g., Falle 1991; Begelman 1996; Kaiser & Alexander 1997).

As seen in Figure 2, one may think this figure seems to support the $v_{\rm HS} = $ const model. However, we should keep in mind the large uncertainty of $v_{\rm HS}$ (§ 2.2). Furthermore, the deceleration may take place via a strong interaction with denser ambient gas in host galaxies, since compact radio sources such as CSOs and MSOs would affect a significant interaction with the surrounding ambient medium as they propagate through it (e.g., Gelderman & Whittle 1994; de Vries et al. 1997; Axon et al. 2000; Gupta et al. 2005; Holt et al. 2008). At present, it is still under debate whether $v_{\rm HS} = $ const is really correct. In order to test the validity of the $v_{\rm HS} = $ const model, we predict the required mass density profile to explain the observed $r_{\rm HS}$-l_h diagram. From equation (2), the relation of $S_v \propto 2 - X(2 - 0.5\alpha) = 0$ is needed for the constant hot spot velocity. By eliminating X, α-dependence of $r_{\rm HS}$ shows

$$r_{\rm HS} \propto l_h^{\alpha/2}. \quad (5)$$

Figure 5 displays the allowed region of the growth rate of cocoon body ($A_c \propto t^X$) plotted versus α (slope of the ambient mass density profile, $\rho_a \propto l_h^{-\alpha}$). The blue-shaded region shows the allowed region given by the best-fit value of the observed $r_{\rm HS}$-l_h relation for the CSO-MSO phase ($l_h < 1$ kpc), i.e., $S_r = 1.34 \pm 0.24$. The red line corresponds to the allowed region obtained for the MSO–FR II phase ($l_h > 1$ kpc), including the fitting errors, i.e., $S_r = 0.44 \pm 0.08$. The black solid line shows $v_{\rm HS} = $ const ($S_v = 0$). The two black dashed lines are relations for the deceleration and acceleration of $v_{\rm HS}$, i.e., $S_v = -1$ and 0.3 (see eq. [2]). The light gray shaded region represents the allowed range of X-parameter derived from comparisons between the KK06 model and relativistic numerical simulations (S02 and PM07). The dark-gray shaded region shows the forbidden region (see § 3). As seen in Figure 5 (*filled triangles and schematic picture*), the constant velocity model can reproduce the observed $r_{\rm HS}$-l_h relation only when the slope of the inner part of the density profile (<1 kpc) is steeper than that of the outer part (>1 kpc), i.e., $\alpha \sim 2.6$ ($l_h <$ 1 kpc) and $\alpha \sim 0.8$ ($l_h > 1$ kpc). However, such a density profile of ambient matter is unrealistic because of the slope of the density profile in many clusters of galaxies $\alpha \approx 1.5 \sim 2$ (e.g., Trinchieri et al. 1986; Mulchaey & Zabludoff 1998; Mathews & Brighenti 2003). Thus, the $v_{\rm HS} = $ const model can be declined.

Similar to the $v_{\rm HS} = $ const model, it is an open question whether the cocoon shape evolves in a self-similar way, i.e., $\mathcal{R} = $ const (De Young 1997; Komissarov & Falle 1998; O'Dea 1998; Carvalho & O'Dea 2002a, 2002b; PM03). Then, we examine whether the $\mathcal{R} = $ const model can reproduce the observed $r_{\rm HS}$-l_h relation. As for the self-similar model, the relation of $S_R \propto X(2.5–0.5\alpha) - 3 = 0$ is needed from equation (4). By eliminating X, $r_{\rm HS}$ can be obtained as

$$r_{\rm HS} \propto l_h^{(\alpha+4)/6}. \quad (6)$$

Figure 6 is the same as Figure 5, but the allowed regions for the aspect ratio $\mathcal{R}$ are plotted. The black solid line denotes $\mathcal{R} =$ const ($S_R = 0$) and the other two black solid lines are the solutions of $S_R = -0.5$ and 0.3. As seen in Figure 6, the self-similar model ($\mathcal{R} = $ const) cannot explain the observed $r_{\rm HS}$-l_h relation because the black solid line does not overlap both blue and red regions. Therefore, the case of $\mathcal{R} = $ const can also be ruled out.

On the whole, two well-known models are not able to explain the observed $r_{\rm HS}$-l_h relation, even if we consider the possibility

[1] The difference from PM07 would come from boundary conditions they adopted. Since they use an open boundary condition in the symmetry plane at the jet basis, this allows the leakage of gas from the boundary (see PM07 for more details). Thus, the hot spot pressure drops faster, and consequently the growth rate of the hot spot radius is higher. These trends for $P_{\rm HS}$ and $r_{\rm HS}$ coincide with the deviations between KK06 and PM07. Concerning the distinction from S02, the effect of relativistic backflow may be a plausible reason considering that the deviation appears only for the evolution of the hot spot radius. If part of jet power is used to fuel the relativistic backflow, its kinetic energy is not available to expand the cocoon sideways. As a result, the growth of head and hot spot radius would be faster in S02 than in KK06. But the deviation (factor 3) is not significant even if we consider the long-term evolution of radio source, e.g., from $\sim 10^{-3}$ to 10^3 kpc. This would imply the relativistic backflow does not have any effect on the cocoon dynamics.

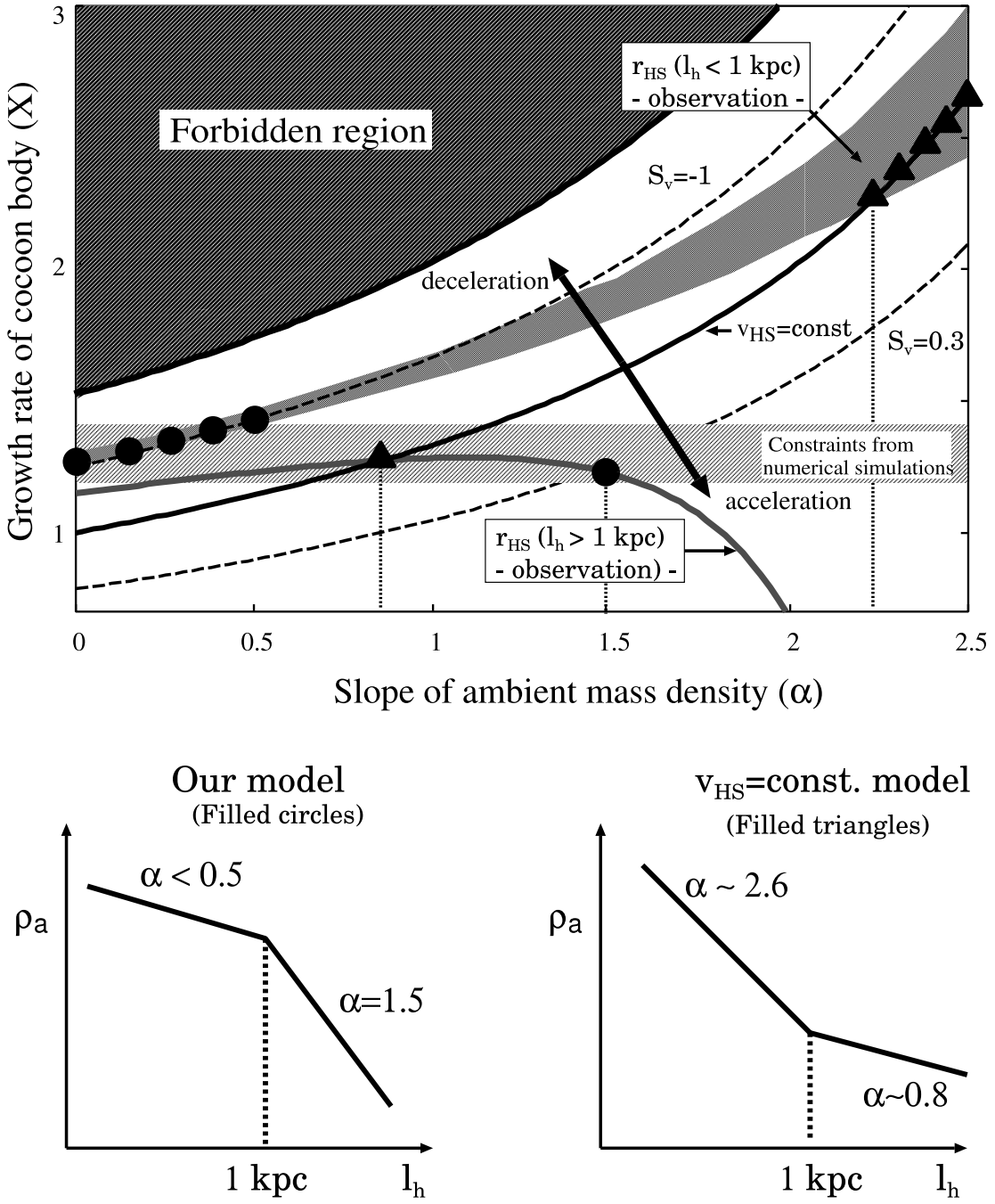

FIG. 5.—Growth rate of the cocoon body ($A_c \propto t^X$) against the value of exponents of the ambient mass density profile ($\rho_a \propto l_h^{-\alpha}$). The shaded region shows the allowed region given by the best-fit value of the observed $r_{\rm HS}$-l_h relation for the CSO-MSO phase ($l_h < 1$ kpc), i.e., $S_r = 1.34 \pm 0.24$. The dark-gray line corresponds to the allowed region obtained for the MSO–FR II phase ($l_h > 1$ kpc), including the fitting errors, i.e., $S_r = 0.44 \pm 0.08$. The black solid line shows $v_{\rm HS} = $ const ($S_v = 0$). The two black dashed lines show the relations of the evolution of hot spot velocity $v_{\rm HS} \propto l_h^{S_v}$. The light-gray shaded region represents the range of X-parameter derived from comparisons between KK06 and numerical simulations. The filled circles show the solutions for our model. We can constrain on he power-law index $\alpha(l_h < 1$ kpc) as $0 \leq \alpha < 0.5$. The filled triangles are solutions for the $v_{\rm HS} =$ const. The predicted ambient mass density profiles are shown. [*See the electronic edition of the Journal for a color version of this figure.*]

that the actual power-law index is steeper than $S_r > 1.34 \pm 0.24$ for $l_h < 1$ kpc (see § 2.1).

4.2. *A New Finding: Deceleration and Acceleration of Hot Spot Velocity*

Here we show an evolutionary track of radio sources to be consistent with the observed evolution of $r_{\rm HS}$ (see Fig. 1). In groups of galaxies and clusters of galaxies ($l_h > 1$ kpc), it is well established that the slope of the density profile is $\alpha \approx 1.5$–2 (e.g., Trinchieri et al. 1986; Mulchaey & Zabludoff 1998; Mathews & Brighenti 2003). We assume $\alpha = 1.5$ for $l_h > 1$ kpc. Comparing the KK06 model with the observed $r_{\rm HS}$-l_h relation (Fig. 1), we can determine (1) the evolution of the advance speed of hot spots, (2) the slope of mass density distribution for $l_h < 1$ kpc, and (3) the evolution of cocoon morphology (see Figs. 5 and 6).

On the evolution of hot spot velocity, we find that the advance speed of the spots and lobes show the deceleration phase (CSO-MSO phase) and the acceleration phase (MSO–FR II phase) as

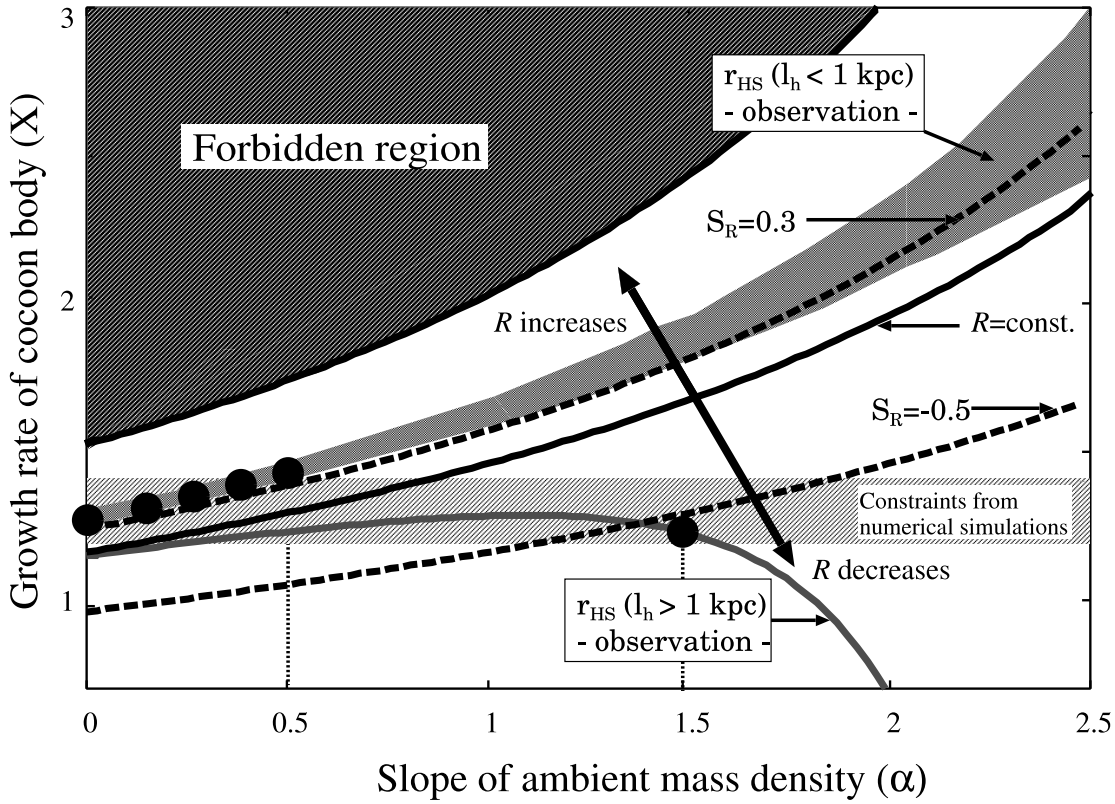

FIG. 6.—Same as Fig. 5, but the black solid line shows $\mathcal{R} = \text{const}$ ($S_R = 0$) and the two black dashed lines show therelations of $S_R = 0.3$ and 0.5, where $\mathcal{R} \propto l_h^{S_R}$. [*See the electronic edition of the Journal for a color version of this figure.*]

follows (see filled circles showing allowed solutions in Fig. 5): In the CSO-MSO phase ($l_h < 1$ kpc), $v_{\rm HS}$ decelerates as

$$v_{\rm HS} \propto l_h^{-1}. \tag{7}$$

In the MSO–FR II phase ($l_h > 1$ kpc), $v_{\rm HS}$ slightly accelerates as

$$v_{\rm HS} \propto l_h^{0.3}. \tag{8}$$

With respect to the CSO-MSO phase ($l_h < 1$ kpc), the flatter density profile ($0 < \alpha \leq 0.5$) is predicted in order to satisfy both the observed $r_{\rm HS}$-l_h diagram and the constraints from numerical simulations (filled circles show the allowed solutions in Fig. 5). The predicted external mass density profile is quite similar to a King-profile distribution, i.e., $\rho_a \propto [1 + (r/r_c)^2]^{0.5\alpha}$, as indicated by X-ray observations of elliptical galaxies (Trinchieri et al. 1986). Typical core radii in giant elliptical galaxies are $r_c = 0.5$–1 kpc (Trinchieri et al. 1986). This coincides with the observational evidence since most CSO/MSO hosts seem to be elliptical galaxies (e.g., O'Dea 1998), although they show the features of distortions and interactions. If we consider the mass density distribution we predicted, the jets propagate through the denser ambient medium during the CSO-MSO phase, compared with the MSO–FR II phase. Then, the interaction between the jets and the ambient medium is stronger in the CSO-MSO phase. This leads to the larger velocity of sideways expansion in order to maintain the energy conservation in the cocoon. Thus, A_h (or $r_{\rm HS}$) grows faster in the early phase of evolution. From the equation of motion along the jet axis (see § 3), it is found that the advance speed of hot spots ($v_{\rm HS}$) is determined by the linear density of the effective working surface, $\rho_a A_h$, i.e., $v_{\rm HS}^2 \propto (\rho_a A_h)^{-1}$. Hence, the deceleration and the acceleration of $v_{\rm HS}$ depends on the change of the power-law index of ambient density profile α in the MSO phase (∼kpc). When $\rho_a A_h$ increases with l_h as the CSO-MSO phase ($\rho_a A_h \propto l_h^2$), the hot spot velocity decelerates. On the other hand, the advance speed accelerates if $\rho_a A_h$ decreases with l_h as the MSO–FR II phase ($\rho_a A_h \propto l_h^{-0.6}$). In the present work, we impose the idea that the evolution of hot spot velocity is mainly determined by the growth of the effective working surface, A_h. Namely, we did not consider the entrainment of the ambient medium in the jets for simplicity (see § 3). We should stress that it is a new aspect that A_h determines the acceleration and deceleration of advance speed of hot spots. Note that the study on the entrainment process on jets is also important and complementary for the deceleration of relativistic jets within ∼1 kpc (e.g., Bicknell 1984; Laing 1993, 1996; De Young 1993, 1997; Komissarov 1994).

Concerning the evolution of cocoon morphology, we show possible solutions (Fig. 6, *filled circles*). As a result, the evolution of a cocoon shape is predicted as follows: In the CSO-MSO phase, the shape of a cocoon is nearly spherical,

$$\mathcal{R} \propto l_h^{0.3}. \tag{9}$$

The cocoon shape is elongated as l_h increases in the MSO–FR II phase as

$$\mathcal{R} \propto l_h^{-0.5}. \tag{10}$$

Hence, the aspect ratio of cocoon in the MSO phase can be close to unity, compared with that in CSOs and FR II sources (see Fig. 7). In the CSO-MSO stage, the hot spot decelerates with l_h, i.e., $v_{\rm HS} \propto l_h^{-1}$, due to the strong interaction with the ambient medium. In order to maintain the energy conservation in the cocoon, $P_c A_c v_{\rm HS} = \text{const}$, and the momentum conservation along

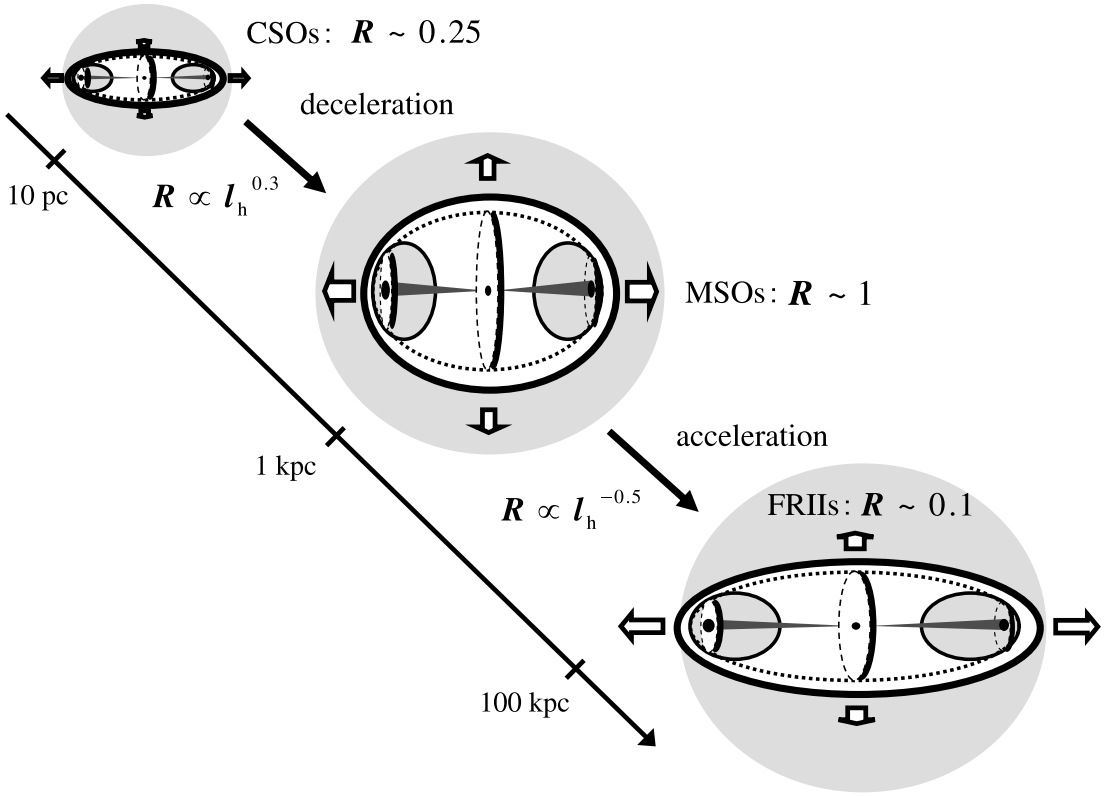

FIG. 7.—Schematic picture of the evolution of a cocoon morphology derived from our predictions (see Fig. 6).

the jet axis, $P_{\rm HS} A_h c = {\rm const}$, the sideways expansion velocity decreases more slowly compared with the advance speed of hot spots, e.g., $v_c \propto l_h^{-0.44}$ for $v_{\rm HS} \propto l_h^{-1}$. Thus, the aspect ratio approaches unity since the aspect ratio of the cocoon can be described as $\mathcal{R} \approx P_c/P_{\rm HS} \propto v_c^2/v_{\rm HS}^2$. In the same manner, it is possible to explain the evolution of the cocoon shape in the MSO-FR II stage, $v_c \propto l_h^{-0.27}$ for $v_{\rm HS} \propto l_h^{0.3}$.

Recently, we have noticed a very interesting radio source (3C 353) whose radio morphology can be well explained by the present model. 3C 353 is an FR II radio galaxy residing on the edge of the cluster and has asymmetric radio lobes, namely, the east lobe is spherical while the west lobe is elongated. Thanks to the new *XMM-Newton* observation, it has been found that the east lobe is located in a denser region than the west lobe (Goodger et al. 2008). From the above discussion, the spherical structure of the east lobe can be understood due to the stronger interaction with the ambient medium than the west lobe. If this is the case, it is predicted that the advance speed of the east lobe and east hot spot is slower than that of the west lobe. In future, the advance speed of the east lobe and hot spot will approach the sound velocity of the ambient medium. Then, the east lobe's radio morphology will change from FR II into FR I type. Such radio galaxies would be observed as hybrid morphology radio sources (HYMORS), which have clear radio lobes with two different morphologies (e.g., Gopal-Krishna & Wiita 2000; Gawroński et al. 2006). In order to understand the origin of HYMORS, i.e., the origin of FR I/FR II dichotomy, it would be important to measure the mass density profile around HYMORS.

5. PREDICTION OF FATE OF CSOs: DEAD OR ALIVE?

In § 4 we found that the observed $r_{\rm HS}$-l_h relation indicates that the advance speed decelerates in the CSO-MSO stage and accelerates in the MSO–FR II stage. However, some CSOs would evolve into some other type of radio source like low-power extended radio galaxies (FR I radio galaxies), since $\leq$10 kpc scale dying MSOs, which do not evolve into FR II radio galaxies, have been discovered (Parma et al. 2007).

Thus, we need to further investigate in this section the fate of CSOs, or which kinds of CSOs can evolve into FR II sources. To this aim, we compare the predicted evolution of $v_{\rm HS}$ with the sound velocity of the ambient medium, c_s, because the cocoon can expand only when $v_{\rm HS} > c_s$. As for the slope of ambient matter density, we assume $\alpha\,(l_h < 1\ {\rm kpc}) = 0$ and $\alpha\,(l_h > 1\ {\rm kpc}) = 1.5$ (see § 4.2). Correspondingly, the behavior of $v_{\rm HS}$ can be determined as $v_{\rm HS} \propto l_h^{-1}$ for $l_h < 1$ kpc and $v_{\rm HS} \propto l_h^{0.3}$ for $l_h > 1$ kpc (see eqs. [7] and [8]). The hot ambient-gas temperature, T_g is measured in the range of $T_g = 5 \times 10^6\ {\rm K} - 2 \times 10^7\ {\rm K}$, i.e., $c_s = (5kT_g/3m_p)^{1/2} \approx 7 \times 10^{-4} c - 1.4 \times 10^{-3} c$, where c_s is the sound velocity of the ambient medium (e.g., Trinchieri et al. 1986), k is the Boltzman constant, and m_p is the proton mass.

Figure 8 shows the evolution of hot spot velocity for three initial advance speeds of the ambient medium with $v_{\rm HS}(l_{h,2{\rm D}}) = 0.01$, 0.1 and 0.5 c, where $l_{h,2{\rm D}} \equiv v_{\rm HS}(l_{h,2{\rm D}}) t_{\rm min}$ is the distance from the core at which the 2D phase (A_h growth phase) starts. Here we suppose $l_{h,2{\rm D}} = 5$ pc from Figure 1.

As seen in Figure 8, we find that CSOs can evolve into FR II sources, passing through MSOs for any l_h when $v_{\rm HS}(l_{h,2{\rm D}})$ is larger than about 0.1 c because of $v_{\rm HS}(l_h) > c_s$. On the other hand, when $v_{\rm HS}(l_{h,2{\rm D}})$ is less than about 0.1 c, $v_{\rm HS}$ is comparable to the sound velocity of hot spots during the CSO-MSO phase ($l_h < 1$ kpc). When $v_{\rm HS}$ equals to c_s, the matter and energy of the cocoon mix with the ambient medium. After that, the cocoon expands subsonically like a sonic boom (Churazov et al. 2000, 2001; Reynolds et al. 2001; Brighenti & Mathews 2002; Zanni et al. 2003). These results indicate that the advance speed of hot spots during the 1D phase (constant A_h) controls the fate of CSOs.

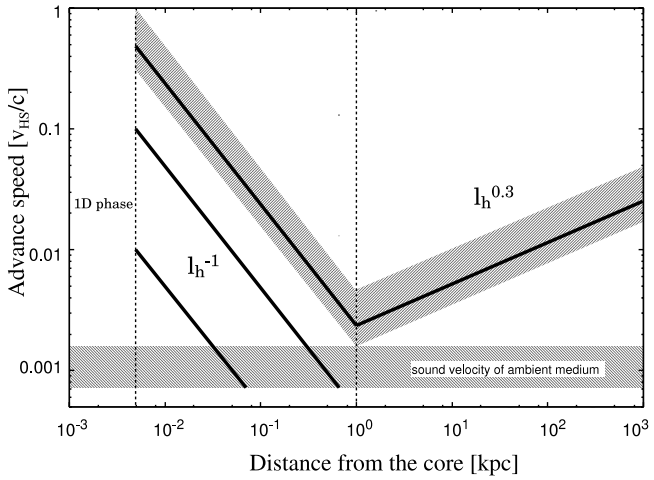

FIG. 8.—Our predictions of evolution of $v_{\rm HS}$, i.e., $v_{\rm HS} \propto l_h^{-1}$ for $l_h < 1$ kpc and $v_{\rm HS} \propto l_h^{0.3}$ for $l_h > 1$ kpc. The black solid lines denote the evolution of $v_{\rm HS}$ for $v_{\rm HS}(l_{h,2D}) = 0.01$, 0.1, and 0.5 c, where $l_{h,2D} = 5$ pc. The upper shaded region represents the evolutionary path from CSOs into FR II radio galaxies. The lower shaded region shows the range of sound velocity of the ambient medium, i.e., $7 \times 10^{-4} c < c_s < 1.4 \times 10^{-3} c$ (5×10^6 K $< T_g < 2 \times 10^7$ K), where T_g is the temperature of the ambient medium. [*See the electronic edition of the Journal for a color version of this figure.*]

Thus, the fate of CSOs can be divided into two cases as follows:

1. *The fate of CSOs with low* $v_{\rm HS}(l_{h,2D}) <\sim 0.1\ c$.—The hot spots velocity is comparable to the sound velocity of ambient matter at the MSO stage (<1 kpc). Consequently, the ambient gas may be heated up since the relativistic plasma within the cocoon leaks into the ambient medium. The cocoon morphology is distorted in the MSO phase. After that, radio sources would expand with the sound velocity. Thus, the evolutionary sequence appears as follows: CSO → MSO → FRI.

2. *The fate of CSO with high* $v_{\rm HS}(l_{h,2D}) >\sim 0.1\ c$.—The CSOs can evolve into FR II sources, passing through MSOs whose cocoon shape is spherical. Namely, the evolutionary sequence is as follows: CSO → MSO → FR II.

The above predicted cocoon morphology of MSOs may coincide with observations in which the fraction of distorted morphology of MSOs is higher than that of CSOs (Saikia et al. 1995; O'Dea 1998; Dallacasa et al. 2002a, 2002b; Parma et al. 2007). Moreover, with respect to case 1, Drake et al. (2004) observed radio-weak CSOs from the *IRAS* survey, then they found that radio-weak CSOs are young ($<10^6$ yr) and show slightly irregular morphology radio sources (also see Kunert-Bajraszewska et al. 2005). Therefore, such radio-weak CSOs may be young counterparts of ~1 kpc scale low-power compact radio sources (Giroletti et al. 2007). Such low-power CSOs might be observed as the dying MSOs (e.g., Parma et al. 2007). As another possibility, low-power CSOs may be the progenitors of FR I radio galaxies because the radio lobes expand with $\approx c_s$, and then the projected linear size of radio sources can reach ~30 kpc ($=10^{-3}\ c \times 10^8$ yr) if the typical age of FR I radio galaxies is $\approx 10^8$ yr (Parma et al. 1999). If this is the case, the origin of the FR I/FR II dichotomy could be related to the difference in initial advance speed of hot spots $v_{\rm HS,1D}$ which depend on L_j and ρ_a (see § 3).

Moreover, these findings impact on AGN feedback associated with AGN jets. The influence of AGN activity on the evolution of the host galaxy is now a hot and timely topic. It has been suggested that the AGN bubbles quench star formation and regulate the SMBH growth, and consequently the local BH-to-bulge relation can be well reproduced (e.g., Silk & Rees 1998; King 2003). However, we should recall that their conclusions rely on the dynamical evolution of AGN bubbles with the constant shock velocity ($v_{\rm HS}$ = const), assuming a singular isothermal hot ambient distribution ($\rho_a \propto r^{-2}$). However, as we mentioned, the constant velocity model does not match with our predictions derived from the actual evolution of young radio sources. Therefore, we must reconsider the conditions that AGN feedback due to AGN jets works effectively. This is left for our future work.

Finally, it is of value to mention what we should do as future observations, to reveal the dynamical evolution of radio sources as follows:

1. We need to evaluate the accurate $v_{\rm HS}$ of MSOs in future VLBI observations, to test the deceleration and acceleration of hot spot velocity. At the same time, it is important to estimate the advance velocity of hot spots for FR II radio galaxies by kinematic studies because most $v_{\rm HS}$ for them have been derived by synchrotron-aging work only.

2. In order to confirm the evolution of the cocoon shape we predict here (see Fig. 7), it is worth systematically measuring the aspect ratio of cocoons for CSOs, MSOs, and FR II radio galaxies. But the emission of the cocoon body is very faint in general due to the synchrotron cooling, and thus it would be hard to assess the clear shape of a cocoon (i.e., A_c) by the present facility. The sensitivity and low-frequency capability of SKA can be used for direct measurement of cocoon morphology, since the cooling effect is smaller at lower frequency. Instead of the direct measurement of the cocoon shape, it is also important to measure the morphology of radio lobes, i.e., $A_h^{1/2}/l_h$ (see Fig. 4) as far as $A_c \propto A_h$ is a reasonable assumption.

3. In the present paper we impose the idea that the initial advance velocity of hot spots, $v_{\rm HS}(l_{h,2D})$, may be interpreted by the differences in total kinetic energy. However, we cannot rule out the possibility that the ambient mass density controls $v_{\rm HS}(l_{h,2D})$. Thus, it is crucial to systematically explore whether there is a significant difference in ambient mass density for CSOs, MSOs, and FR II radio galaxiess. For this purpose, the search for cold gas via molecular gas and 21 cm H I is very useful using future facilities with high spatial resolution such as ALMA and SKA. At the same time, the study of diffuse hot gas will be also important using future X-ray satellites with high sensitivity and high spatial resolution such as *XEUS* (*X-Ray Evolving Universe Spectrometer*) and *Constellation-X*.

4. In order to reveal the end of the 1D phase of hot spot evolution, it is necessary to discover and elucidate the candidates for ultracompact symmetric radio sources (e.g., $l_h < 5$ pc) such as high-frequency peakers (HFPs). These have been intensively observed, and a growing number of the sources are being detected (e.g., Dallacasa et al. 2000; Tinti et al. 2005; Orienti et al. 2007), using high-resolution VLBI such as VSOP-2 (see also Snellen 2008). This is very important not only to predict the fate of CSOs, as we mentioned, but also to reveal the physical conditions for the transitions from 1D phase to 2D phase.

5. It is worth exploring whether radio-weak CSOs, including radio-quiet AGNs (Seyfert galaxies and radio-quiet quasars) follow the same $r_{\rm HS}$-l_h diagram. The present model predicts that the observed $r_{\rm HS}$-l_h relation of bright radio sources holds radio-weak sources as far as the AGN jets are composed of the relativistic plasma. So far, it has been very difficult to measure the hot spot properties (e.g., size and velocity) because of the faintness of low-powered jet sources. However, future low-frequency radio telescopes (e.g., LOFAR and SKA) are ideal tools for understanding

the dynamical evolution of radio-weak sources from the point of view of sensitivity and the low-frequency capability.

6. SUMMARY

We have investigated the physical relationship between CSOs, MSOs, and FR II radio galaxies, together with the coevolution model of hot spots and a cocoon (KK06) and the observation reflecting the dynamical evolution of radio sources. For a larger sample of radio sources than previous work (JS00; PM03), we find that the evolution of the hot spot radius clearly changes at $l_h \sim 1$ kpc, even after we carefully exclude the observational bias. Based on these observational characteristics of hot spots, we investigate the evolutionary track of extragalactic radio galaxies. The main results of the present work are summarized as follows:

1. We test two well-known evolution models of radio sources, i.e., "the constant velocity" model and "the constant aspect ratio" model. Since the mass density profile of the ambient matter shows unrealistic behavior, i.e., the derived power-law index ($\alpha \approx 0.8$) is shallower than $\alpha = 1.5$–2 in groups of galaxies and clusters of galaxies, the constant velocity model can be ruled out. In the case of the self-similar model, it turns out that the constant aspect ratio model cannot reproduce the observed $r_{\rm HS}$-l_h relation. Therefore, the case of constant aspect ratio can also be declined.

2. We investigate the evolution of hot spot velocity to reproduce the observed $r_{\rm HS}$-l_h relation. As a result, we find that the advance speed of hot spots and lobes strongly decelerate when the jets pass through the ambient medium in host galaxies (i.e., the CSO-MSO phase), while the jets slightly accelerate outside host galaxies (i.e., the MSO–FR II phase). Recent observation shows that a possible correlation between the outflow velocity of the ionized gas and l_h might indicate a possible deceleration of the jets as they pass through the host galaxy (Labiano 2008). This trend seems to be consistent with the preferred model, although the available data is not enough to compare with our prediction. Furthermore, we can constrain the allowed value of α as $0 \leq \alpha < 0.5$ for $l_h < 1$ kpc. The main origin of the deceleration and acceleration of hot spots is the change in power-law index of ambient density distribution at $\sim$1 kpc. It is worth emphasizing again that the advance speed of hot spots is determined by the growth of the cocoon head, which is a new aspect of the deceleration and acceleration of relativistic jets.

3. It is also found that the cocoon shape of MSOs becomes spherical or disrupted, while the cocoon morphology of CSOs and FR II radio galaxies is elongated. The radio image of MSOs seems to be consistent with our prediction (Dallacasa et al. 2002a, 2002b). However, the emission of the cocoon is generally very faint due to the synchrotron cooling, and thus it is quite difficult to observe it using present facilities. Thus, it is of value to systematically measure the aspect ratio (or the morphology of radio lobes) for CSOs, MSOs, and FR II radio galaxies using future low-frequency radio telescopes (e.g., LOFAR and SKA).

4. We predict the fate of CSOs, comparing the advance speed of hot spots with the sound velocity of the ambient medium. Only CSOs whose initial advance speed is higher than about 0.1 c can be progenitors of powerful FR II radio galaxies. It would be in agreement with the observation which the fraction of FR II radio galaxiesis less than that of CSOs. Moreover, the fate of CSOs would be closely related to the FR I/FR II dichotomy and AGN feedback, which we will discuss in an upcoming paper.

We would like to thank A. Cellotti, I. A. G. Snellen, L. Danese, M. Nakamura, S. Inoue, S. Jeyakumar, and T. Nagao for fruitful discussions. We also thank an anonymous referee for useful comments. N. K. is financially supported by the Japan Society for the Promotion of Science (JSPS) through the JSPS Research Fellowship for Young Scientists. M. K. acknowledges the Grant-in-Aid for Scientific Research of the Japanese Ministry of Education, Culture, Sports, Science and Technology, No. 14079025. This research has made use of the NASA/IPAC Extragalactic Database (NED), which is operated by the Jet Propulsion Laboratory, California Institute of Technology, under contract with the National Aeronautics and Space Administration.

REFERENCES

Alexander, P. 2000, MNRAS, 319, 8
Alexander, P., Brown, M. T., & Scott, P. F. 1984, MNRAS, 209, 851
Alexander, P., & Leahy, J. P. 1987, MNRAS, 225, 1
Asada, K., Kameno, S., Shen, Z.-Q., Horiuchi, S., Gabuzda, D. C., & Inoue, M. 2006, PASJ, 58, 261
Axon, D. J., et al. 2000, AJ, 120, 2284
Begelman, M. C. 1996, in Cygnus A: Study of a Radio Galaxy, ed. C. L. Carilli & D. E. Harris (Cambridge: Cambridge Univ. Press), 209
Begelman, M. C., & Cioffi, D. F. 1989, ApJ, 345, L21
Bicknell, G. V. 1984, ApJ, 286, 68
Blandford, R. D., & Rees, M. J. 1974, MNRAS, 169, 395
Bridle, A. H., Hough, D. H., Lonsdale, C. J., Burns, J. O., & Laing, R. A. 1994, AJ, 108, 766
Brighenti, F., & Mathews, W. 2002, ApJ, 574, L11
Carilli, C. L., Perley, R. A., Dreher, J. W., & Leahy, J. P. 1991, ApJ, 383, 554
Carvalho, J. C. 1985, MNRAS, 215, 463
Carvalho, J. C., & O'Dea, C. P. 2002a, ApJS, 141, 337
———. 2002b, ApJS, 141, 371
Churazov, E., et al. 2000, A&A, 356, 788
———. 2001, ApJ, 554, 261
Dallacasa, D., Fanti, C., Giacintucci, S., Stanghellini, C., Fanti, R., Gregorini, L., & Vigotti, M. 2002a, A&A, 389, 126
Dallacasa, D., Stanghellini, C., Centonza, M., & Fanti, R. 2000, A&A, 363, 887
Dallacasa, D., Tinti, S., Fanti, C., Fanti, R., Gregorini, L., Stanghellini, C., & Vigotti, M. 2002b, A&A, 389, 115
de Vries, W. H., Barthel, P. D., & O'Dea, C. P. 1997, A&A, 321, 105
de Vries, W. H., O'Dea, C. P., Baum, S. A., & Barthel, P. D. 1999, ApJ, 526, 27
De Young, D. S. 1993, ApJ, 405, L13
———. 1997, ApJ, 490, L55
Di Matteo, T., Springel, V., & Hernquist, L. 2005, Nature, 433, 604
Drake, C. L., Bicknell, G. V., McGregor, P. J., & Dopita, M. A. 2004, AJ, 128, 969
Falle, S. A. E. G. 1991, MNRAS, 250, 581
Fanti, C., Fanti, R., Parma, P., Schilizzi, R. T., & van Breugel, W. J. M. 1985, A&A, 143, 292
Fanti, C., et al. 1995, A&A, 302, 317
Fernini, I., Burns, J. O., Bridle, A. H., & Perley, R. A. 1993, AJ, 105, 1690
Gawroński, M. P., Marecki, A., Kunert-Bajraszewskam, M., & Kus, A. J. 2006, A&A, 447, 63
Gelderman, R., & Whittle, M. 1994, ApJS, 91, 491
Gilbert, G. M., Riley, J. M., Hardcastle, M. J., Croston, J. H., Pooley, G. G., & Alexander, P. 2004, MNRAS, 351, 845
Giroletti, M., et al. 2003, A&A, 399, 889
———. 2007, preprint (arXiv: 0707.3516)
Goodger, J. L., Hardcastle, M. J., Croston, J. H., Kassim, N. E., & Perley, R. A. 2008, MNRAS, 386, 337
Gopal-Krishna, & Wiita, P. J. 2000, A&A, 363, 507
Granato, G. L., et al. 2004, ApJ, 600, 580
Gugliucci, N. E., Taylor, G. B., Peck, A. B., & Giroletti, M. 2005, ApJ, 622, 136
———. 2007, ApJ, 661, 78
Gupta, N., Salter, C. J., & Saikia, D. J. 2005, MNRAS, 361, 451
Hardcastle, M. J., Alexander, P., Pooley, G. G., & Riley, J. M. 1997, MNRAS, 288, 859
———. 1998, MNRAS, 296, 445
Holt, J., Tadhunter, C. N., & Monganti, R. 2008, MNRAS, in press (arXiv: 0802.1444)
Ito, H., et. al. 2008, ApJ, submitted
Jamrozy, M., Machalski, J., Mack, K.-H., & Klein, U. 2005, A&A, 433, 467

Jeyakumar, S., & Saikia, D. J. 2000, MNRAS, 311, 397 (JS00)
Kaiser, C. R., & Alexander, P. 1997, MNRAS, 286, 215
Kawakatu, N., & Kino, M. 2006, MNRAS, 370, 1513 (KK06)
Kawata, D., & Gibson, B. K. 2005, MNRAS, 358, L16
Kharb, P., O'Dea, C. P., Baum, S. A., Daly, R. A., Mory, M. P., Donahue, M., & Guerra, E. J. 2008, ApJS, 174, 74
King, A. 2003, ApJ, 596, L27
Kino, M., & Kawakatu, N. 2005, MNRAS, 364, 659 (KK05)
Kino, M., & Kawakatu, N., & Ito, H. 2007, MNRAS, 376, 1630
Klein, U., Mack, K.-H., Gregorini, L., & Parma, P. 1995, A&A, 303, 427
Komissarov, S. S. 1994, MNRAS, 269, 394
Komissarov, S. S., & Falle, S. A. E. G. 1998, MNRAS, 297, 1087
Kunert-Bajraszwska, M., Marecki, A., Thomasson, P., & Spencer, R. E. 2005, A&A, 440, 93
Labiano, A. 2008, A&A, 488, L59
Laing, R. A. 1993, in Astrophysical Jets, ed. D. Burgarella, M. Livio, & C. O'Dea (Cambridge: Cambridge Univ. Press), 95
———. 1996, in IAU Symp. 175, Extragalactic Radio Sources, ed. R. D. Eckers, C. Fanti, & L. Padrielli (Dordrecht: Kluwer), 147
Liu, R., Pooley, G., & Riley, J. M. 1992, MNRAS, 257, 545
Luo, W.-F., et al. 2007, Chinese J. Astron. Astrophys., 7, 611
Mack, K.-H., Klein, U., O'Dea, C. P., Willis, A. G., & Saripalli, L. 1998, A&A, 329, 431
Maness, H. L., Taylor, G. B., Zavala, R. T., Peck, A. B., & Pollack, L. K. 2004, ApJ, 602, 123
Marecki, A., Spencer, R. E., & Kunert, M. 2003, Publ. Astron. Soc. Australia, 20, 46
Mathews, W. G., & Brighenti, F. 2003, ARA&A, 41, 191
Mizuta, A., Yamada, S., & Takabe, H. 2004, ApJ, 606, 804
Mulchaey, J. S., & Zabludoff, A. I. 1998, ApJ, 496, 73
Murgia, M., et al. 1999, A&A, 345, 769
Murray, N., Quataert, E., & Thompson, T. A. 2005, ApJ, 618, 569
Nagai, H., 2007, Ph.D. thesis, Graduate University for Advanced Studies (Sokendai)
Nagai, H., Inoue, M., Asada, K. Kameno, S., & Doi, A. 2006, ApJ, 648, 148
O'Dea, C. P. 1998, PASP, 110, 493
O'Dea, C. P., et al. 2002, AJ, 123, 2333
Okamoto, T., Nemmen, R. S., & Bower, R. G. 2008, MNRAS, 385, 161
Orienti, M., Dallacasa, D., & Stanghellini, C. 2007, A&A, 475, 813
Owsianik, I., & Conway, J. E. 1998, A&A, 337, 69
Owsianik, I., Conway, J. E., & Polatidis, A. G. 1998, A&A, 336, L37
Parma, P., Murgia, M., Morganti, R., Capetti, A., de Ruiter, H. R., & Fanti, R. 1999, A&A, 344, 7
Parma, P., et al. 2007, A&A, 470, 875
Perley, R. A. 1999, in ASP Conf. Ser. 180, Synthesis Imaging in Radio Astronomy II, ed. G. B. Tayor, C. R. Carilli, & R. A. Perly (San Francisco: ASP), 275
Perucho, M., & Martí, J. M. 2002, ApJ, 568, 639
———. 2003, Publ. Astron. Soc. Australia, 20, 94 (PM03)
———. 2007, MNRAS, 382, 526 (PM07)
Phillips, R. B., & Mutel, R. L. 1982, A&A, 106, 21
Polatidis, A. G., & Conway, J. E. 2003, Publ. Astron. Soc. Australia, 20, 69
Readhead, A. C. S., Taylor, G. B., Xu, W., Pearson, T. J., Wilkinson, P. N., & Polatidis, A. G. 1996a, ApJ, 460, 612
Readhead, A. C. S., et al. 1996b, ApJ, 460, 634
Reynolds, C. S., Heinz, S., & Begelman, M. C. 2001, ApJ, 549, L179
Saikia, D. J., et al. 1995, MNRAS, 276, 1215
Sanghera, H. S., Saikia, D. J., Luedke, E., Spencer, R. E., Foulsham, P. A., Akujor, C. E., & Tzioumis, A. K. 1995, A&A, 295, 629
Scheck, L., et al. 2002, MNRAS, 331, 615 (S02)
Scheuer, P. A. 1974, MNRAS, 166, 513
Schoenmakers, A. P., de Bruyn, A. G., Röttgering, H. J. A., & van der Laan, H. 2000, MNRAS, 315, 395
Silk, J., & Rees, M. J. 1998, A&A, 331, L1
Spencer, R. E., McDowell, J. C., Charlesworth, M., Fanti, C., Parma, P., & Peacock, J. A. 1989, MNRAS, 240, 657
Snellen, I. A. G. 2008, in ASP Conf. Ser., Approaching Micro-Arcsecond Resolution with VSOP-2: Astrophysics and Technologies, ed. Y. Hagiwara et al. (San Francisco: ASP), in press (arXiv: 0802.1976)
Snellen, I. A. G., Schilizzi, R. T., & van Langevelde, H. J. 2000, MNRAS, 319, 429
Taylor, G. B., Marr, J. M., Pearson, T. J., & Readhead, A. C. S. 2000, ApJ, 541, 112
Taylor, G. B., & Vermeulen, R. C. 1997, ApJ, 485, L9
Tinti, S., Dallacasa, D., de Zotti, G., Celotti, A., & Stanghellini, C. 2005, A&A, 432, 31
Trinchieri, G., Fabbiano, G., & Canizares, C. R. 1986, ApJ, 310, 637
Tschager, W., et al. 2000, A&A, 360, 887
Tzioumis, A. K., et al. 1989, AJ, 98, 36
van Breuge, l W. J. M., Miley, G. K., & Heckman, T. A. 1984, AJ, 89, 5
Wang, W.-H., Hong, X.-Y., & An, T. 2003, Chinese J. Astron. Astrophys., 3, 505
Wilkinson, P. N., et al. 1994, ApJ, 432, L87
Wyithe, S., & Loeb, A. 2003, ApJ, 595, 614
Zanni, C., et al. 2003, A&A, 402, 949